Key Points:
- Climate forcing and spatial and temporal variability of North American ecosystem
- Evaluate a 2-D biophysical model/dynamic vegetation using satellite data
- Mechanisms affecting vegetation/climate interaction

Correspondence to:
Y. Xue,
yxue@geog.ucla.edu

Investigation of North American vegetation variability under recent climate: A study using the SSiB4/TRIFFID biophysical/dynamic vegetation model

Zhengqiu Zhang[1,2,3], Yongkang Xue[1,4], Glen MacDonald[1], Peter M. Cox[5], and G. James Collatz[6]

[1]Department of Geography, University of California, Los Angeles, California, USA, [2]Chinese Academy of Meteorological Sciences, Beijing, China, [3]Institute of Atmospheric Environment, China Meteorological Administration, Shenyang, China, [4]Department of Atmospheric Sciences, University of California, Los Angeles, California, USA, [5]College of Engineering, Mathematics and Physical Science, University of Exeter, Exeter, UK, [6]NASA Goddard Space Flight Center, Greenbelt, Maryland, USA

Abstract Recent studies have shown that current dynamic vegetation models have serious weaknesses in reproducing the observed vegetation dynamics and contribute to bias in climate simulations. This study intends to identify the major factors that underlie the connections between vegetation dynamics and climate variability and investigates vegetation spatial distribution and temporal variability at seasonal to decadal scales over North America (NA) to assess a 2-D biophysical model/dynamic vegetation model's (Simplified Simple Biosphere Model version 4, coupled with the Top-down Representation of Interactive Foliage and Flora Including Dynamics Model (SSiB4/TRIFFID)) ability to simulate these characteristics for the past 60 years (1948 through 2008). Satellite data are employed as constraints for the study and to compare the relationships between vegetation and climate from the observational and the simulation data sets. Trends in NA vegetation over this period are examined. The optimum temperature for photosynthesis, leaf drop threshold temperatures, and competition coefficients in the Lotka-Volterra equation, which describes the population dynamics of species competing for some common resource, have been identified as having major impacts on vegetation spatial distribution and obtaining proper initial vegetation conditions in SSiB4/TRIFFID. The finding that vegetation competition coefficients significantly affect vegetation distribution suggests the importance of including biotic effects in dynamical vegetation modeling. The improved SSiB4/TRIFFID can reproduce the main features of the NA distributions of dominant vegetation types, the vegetation fraction, and leaf area index (LAI), including its seasonal, interannual, and decadal variabilities. The simulated NA LAI also shows a general increasing trend after the 1970s in responding to warming. Both simulation and satellite observations reveal that LAI increased substantially in the southeastern U.S. starting from the 1980s. The effects of the severe drought during 1987–1992 and the last decade in the southwestern U.S. on vegetation are also evident from decreases in the simulated and satellite-derived LAIs. Both simulated and satellite-derived LAIs have the strongest correlations with air temperature at northern middle to high latitudes in spring reflecting the effect of these climatic variables on photosynthesis and phenological processes. Meanwhile, in southwestern dry lands, negative correlations appear due to the heat and moisture stress there during the summer. Furthermore, there are also positive correlations between soil wetness and LAI, which increases from spring to summer. The present study shows both the current improvements and remaining weaknesses in dynamical vegetation models. It also highlights large continental-scale variations that have occurred in NA vegetation over the past six decades and their potential relations to climate. With more observational data availability, more studies with different models and focusing on different regions will be possible and are necessary to achieve comprehensive understanding of the vegetation dynamics and climate interactions.

1. Introduction

The climate exerts dominant control on the spatial distribution of the major vegetation types on a global scale [e.g., *MacDonald*, 2002; *Woodward et al.*, 2004], and vegetation in turn can influence climate, both directly through surface energy and water budget via exchanges of radiation, heat, water, and momentum [e.g., *Xue*, 1997; *Xue et al.*, 2010; *Bounoua et al.*, 2010] and indirectly through biogeochemical processes via their effects on atmospheric CO_2 [e.g., *Cox et al.*, 2000; *Kaufmann et al.*, 2003; *Beringer*, 2010]. While the modeled effects of vegetation on climate with specified land surface vegetation conditions have been

extensively investigated, as indicated above, the understanding of the broad range of vegetation response to climate variability and change is less clearly developed.

In recent decades, the scientific community has attempted to quantify the missing climate-vegetation feedbacks by incorporating dynamic vegetation models (DVMs) within climate models, such that the land cover is treated as an interactive element [e.g., *Dickinson et al.*, 1998; *Foley et al.*, 1998; *Friend et al.*, 1998; *Daly et al.*, 2000; *Cox et al.*, 2001; *Sitch et al.*, 2003; *Delire et al.*, 2004; *Wang et al.*, 2004; *Crucifix et al.*, 2005; *Krinner et al.*, 2005; *Zeng et al.*, 2005; *Bonan and Levis*, 2006; *Scheller et al.*, 2007]. While DVMs have demonstrated their utility in paleoclimate studies [e.g., *Kutzbach et al.*, 1996; *Claussen and Gayler*, 1997], in which temporal scales are consistent with most DVMs' original design, a few sensitivity studies suggest that two-way land/atmosphere feedbacks, which the DVMs are intended to simulate, may also be important in climate studies even at seasonal/interannual/decadal scales. For example, *Lu et al.* [2001] used the coupled Regional Atmospheric Modeling System and CENTURY ecosystem model with a specified climate-leaf area index (LAI) curve to study regional-scale two-way interactions between the atmosphere and biosphere in the central United States. The results show that seasonal vegetation phenological variation strongly influences regional climate patterns through its control over land surface water and energy exchange. The coupled model captures the key aspects of weekly, seasonal, and annual feedbacks between the atmospheric and ecological systems. In another study, using a prognostic LAI parameterization, which depends on temperature and soil water, *Levis and Bonan* [2004] found a dynamic coupling between the atmosphere and vegetation, in which the observed reduction in the springtime warming trend over northern Europe, central Canada, and eastern China occurred only when photosynthesis, stomatal conductance, and leaf emergence were synchronized with the surface climate; the prescribed LAI failed to simulate this phenomenon. In another study on soil moisture-vegetation-precipitation feedback over the North American (NA) summer with/without dynamic vegetation feedbacks [*Kim and Wang*, 2012], it was found that with vegetation being fixed, there was no clear signal in responding to dry soil moisture anomalies (SMAs). In contrast, with dynamic vegetation feedback included, the simulation showed a positive feedback between vegetation and precipitation under dry SMA conditions.

Meanwhile, studies have also investigated relationships between vegetation and climate variability over NA with statistical techniques applied to observed climate data and satellite-derived vegetation data. These studies show significant relationships between large-scale climatic conditions and remotely sensed vegetation variables [e.g., *Zhou et al.*, 2003; *Alessandri and Navarra*, 2008; *Rehfeldt et al.*, 2006; *Liu et al.*, 2006; *Notaro et al.*, 2006; *Wang et al.*, 2006; *Potter et al.*, 2008; *Wang et al.*, 2011; *Zeng et al.*, 2013]. All of these studies show the importance of including the DVM in land/atmosphere interaction studies at seasonal, interannual, and decadal scales. However, although the DVMs have shown the promise in climate studies as discussed above, it still remains a great challenge to properly simulate the vegetation/climate interactions at different scales due to the uncertainty in correctly modeling ecosystem processes with adequate parameterization [e.g., *Zaehle et al.*, 2005].

Recent analyses based on the multi-DVM simulations show substantial deficiency in DVMs in decadal climate studies. Using the Global Inventory Monitoring and Modeling System (GIMMS) [*Zhu et al.*, 2013] leaf area index (LAI) product from the period July 1981 to December 2010 at a 15 day frequency, several DVMs' performance in offline experiments as well as when coupled with the general circulation models (GCMs) in the Coupled Model Intercomparison Project Phase 5 (CMIP5) simulations over the high-latitude Northern Hemisphere have been evaluated [*Murray-Tortarolo et al.*, 2013; *Anav et al.*, 2013]. LAI, defined as the one-sided green leaf area per unit ground area, is an important vegetation variable because it affects the radiative transfer process within the canopy as well as evapotranspiration and photosynthesis processes and consequently modulates near-surface climate and atmospheric circulations. It is found that all the models in both offline and coupled modes greatly overestimate the mean LAI, length of the growing season, and seasonal amplitudes, particularly over the boreal forest. Because LAI is an important vegetation parameter and LAI and associated vegetation biogeophysical processes (BGP) have important effects on global and regional climate simulation [e.g., *Kang et al.*, 2007; *Li et al.*, 2007; *Xue et al.*, 2010], the deficiency in the mean LAI and its seasonality would have important implications for climate change study. *Murray-Tortarolo et al.* [2013] have found that all these coupled CMIP5 GCMs/DVMs except one, which properly simulated LAI, produced substantially higher precipitation compared with observation. They also found that models that included more plant functional types (PFTs) and those that calculate their phenology based on temperature rather than with complex photosynthetic modules

produced better results. Moreover, they found that "models with prescribed vegetation more closely match observations than those that simulate it dynamically." Since the dynamic simulation of PFT distribution is the core of the DVMs, these discoveries indicate an important deficiency in today's DVMs.

Lack of validation data has hampered efforts in evaluating DVMs' performance in relation to seasonal to decadal variability and their role in climate variability. New high-resolution satellite data are now available, covering a period of several decades and providing an opportunity to validate DVM estimates. In past decades, validation and calibration using observational data, especially through model intercomparison projects such as the Project for Intercomparison of Land surface Parameterization Schemes (PILPS) [*Henderson-Sellers et al.*, 1993] and the Model Parameter Estimation experiment [*Duan et al.*, 2006; *Di et al.*, 2014], have proved to be extremely helpful for the development of land models. We believe that these model validation, calibration, and intercomparison approaches are also important for the development of satisfactory DVMs. In this study, we will demonstrate that after improvement in parameterizations and important parameter settings using observational data over NA, a DVM model with few carefully selected plant functional types (PFTs) is able to produce realistic vegetation results when compared with satellite products. This study contributes to the necessary steps of conducting comprehensive investigations on how plant functional and/or physiological characteristics affect the spatial distribution and competition of plant functional types (PFTs). It also highlights the value of applying large-scale satellite-derived products to evaluate the DVM-simulated spatial distribution and temporal variability. This ultimately increases our understanding of the BGP mechanisms at work, especially how vegetation responds to soil wetness and surface air temperature under different conditions.

In this study, a biophysical/dynamic vegetation model, Simplified Simple Biosphere Model version 4, coupled with the Top-down Representation of Interactive Foliage and Flora Including Dynamics Model (SSiB4/TRIFFID) [*Xue et al.*, 1991; *Cox et al.*, 2001; *Zhan et al.*, 2003], is used to investigate the response of vegetation processes to climate variability in NA and uncertainty in the parameterization and/or parameters. In previous studies (as discussed above), either the validation of simulated LAI or climate/NDVI (Normalized Difference Vegetation Index) relationship was the only focus. This study focuses on four aspects: (1) the production of initial vegetation conditions under current climate for long-term DVM simulation; (2) the ability of this coupled model to produce proper spatial vegetation distributions; (3) the ability to reproduce vegetation seasonal, interannual, and decadal variabilities; and (4) the ability to elucidate the relationships of the spatiotemporal variability of the vegetation with climate and surface conditions. In section 2, we will present the model, the data, and the general methodology for this study. Section 3 will present the results of the quasi-equilibrium vegetation production as vegetation initial conditions for long-term simulation and the important factors affecting the quasi-equilibrium vegetation condition. In section 4, the spatial and temporal variability of the NA vegetation is investigated by analyzing and comparing model simulation results with satellite-derived products. Finally, we analyze the relationships between LAI and climate/surface condition based on both observation and model simulations.

2. Model, Data Sets, and Methodology

2.1. General Approaches of This Study

A coupled biophysical/dynamic vegetation model SSiB4/TRIFFID is applied for this study, and the climate forcing from 1948 to 2008 over NA is used to drive the SSiB4/TRIFFID to produce NA vegetation conditions. The satellite-derived products are used to validate and calibrate the model to produce proper vegetation spatial distribution and temporal variability. Since the DVMs take a long time to spin-up, an approach to obtain the 1948 initial vegetation condition, which would not cause severe spin-up for the long-term simulation, is investigated. The results from this study show the substantial effects of climate on the model-produced vegetation distribution; it is important to evaluate whether the model produced a valid climate/vegetation relationship. Therefore, the observed and simulated relationships between these two components are investigated, which not only provides another way to evaluate the model results but also help understand the mechanisms at work.

2.2. Brief Description of SSiB4/TRIFFID

SSiB4/TRIFFID is based on the balance of energy cycle, water cycle, and carbon cycle at the terrestrial surface and has been tested for several sites with different climate and land cover conditions [*Xue et al.*, 1991; *Cox et al.*, 2001; *Zhan et al.*, 2003]. The SSiB4/TRIFFID has been validated with 13 observational data sets from

different latitudes and landform conditions, including Sahel savanna and shrubs, Amazon tropical rainforest, Alaskan tundra, and boreal forest. In addition to vegetation properties, the observed surface latent heat, sensible heat fluxes, and carbon flux, whenever available, are also used for evaluation. In general, the model is able to reasonably simulate the seasonal variability, with some bias in the diurnal variation at some sites. The results in these site experiments provide very useful information for this study [*Xue et al.*, 2006].

SSiB4 provides estimates of net plant photosynthesis assimilation rate, autotrophic respiration, and other surface conditions, such as soil moisture and canopy temperature for TRIFFID. TRIFFID calculates vegetation parameters such as plant height and LAI for SSiB4. The SSiB4/TRIFFID model involves a dynamic competition mechanism between different PFTs for their growth and dominance. It categorizes global vegetation into six major PFTs, i.e., broadleaf trees, needleleaf trees, C3 grasses, C4 plants, shrubs, and tundra dwarf shrubs; it also includes bare land.

2.3. Data Sets

2.3.1. Forcing Data

The Princeton global meteorological data set for land surface modeling [*Sheffield et al.*, 2006] is used as the forcing for this study, which is constructed by combining a suite of global observation-based data sets with the National Centers for Environmental Prediction/National Center for Atmospheric Research reanalysis data starting from 1948. The spatial resolution is $1° \times 1°$, and the temporal resolution is 3 h. The data set includes surface air temperature, pressure, specific humidity, wind speed, downward short-wave radiation flux, downward long-wave radiation flux, and precipitation. We have also produced a climate forcing data set with a 3 h interval by averaging all 3 h Princeton data from 1948 to 2008. This annual climate data set has diurnal and seasonal variation and will be used for production of initial vegetation conditions.

2.3.2. Satellite-Derived Data

Satellite-derived vegetation products from different sources will be used to evaluate the model-generated vegetation classification over NA, including Global Land Cover (GLC) 2000 [*Latifovic et al.*, 2002; *Mayaux et al.*, 2004], which uses satellite data of the year 2000 from Pour l'Observation de la Terre at a spatial resolution of about 1000 m, and the Moderate Resolution Imaging Spectroradiometer (MODIS) Land Cover Type Climate Modeling Grid product [*Loveland et al.*, 1999; *Friedl et al.*, 2010], which includes International Geosphere-Biosphere Programme (IGBP), University of Maryland, College Park (UMD), and Science Data Set classification schemes at 0.5° (~500 m) spatial resolution. Among them, IGBP and UMD are more comprehensive. After calculating the dominant vegetation types at 1° resolution from the UMD and the IGBP vegetation coverage, it is found that they are quite similar over NA. Since IGBP data also include land ice, we use IGBP for our model validation.

More relevant to the seasonal, interannual, and decadal variability are the LAI products. Two widely used LAI products are used as references for this study. They are the Fourier-Adjusted, Sensor and Solar zenith angle corrected, Interpolated, Reconstructed (FASIR) [*Los et al.*, 2000] data set from 1982 to 1998 and the Global Inventory Monitoring and Modeling System (GIMMS) [*Pinzon et al.*, 2005; *Zhu et al.*, 2013] Boston University (GIMMSBU) LAI from 1981 to 2011. These global biophysical land surface data sets are at 0.25° spatial and monthly temporal resolutions. The FASIR data set includes LAI, vegetation coverage, and the fraction of photosynthetically active radiation absorbed by vegetation.

The FASIR products were generated from the Pathfinder data set with added corrections to account for the surface bidirectional reflectance distribution function, some atmospheric effects, and stratospheric aerosols. The GIMMS Normalized Difference Vegetation Index (NDVI) product uses the original raw advanced very high resolution radiometer rather than the Pathfinder corrected bands. Due to the different algorithms used to convert NDVI to LAI, the individual unique characteristics of each NDVI data set carry through to the LAI. After subtracting the values from seasonal mean, these two data sets show different variability. The long-term trend is more significant and variances are larger in FASIR than in GIMMSBU LAI [*Kang et al.*, 2007]. Since these two data sets provide invaluable surface vegetation information and provide a measure of the uncertainty in the satellite products, we will use both to evaluate model products.

The GLC2000 and MODIS IGBP and SSiB4/TRIFFID have different classification schemes. The SSiB4/TRIFFID consists of only primary land cover types, while both GLC2000 and MODIS IGBP have more sublevel classes. For easy comparison of the distribution of dominant vegetation types with different products, we hierarchically combined the GLC2000 and the MODIS IGBP classifications to SSiB4/TRIFFID PFTs (Table 1).

**Table 1.** Comparisons of Different Land Cover Type Classifications

No.	SSiB4/TRIIFID	GLC2000 Class	GLC2000 Description	MODIS IGBP Class	MODIS IGBP Description
1	Broadleaf tree	1	Tropical or subtropical broadleaved evergreen forest—closed canopy	2	Evergreen broadleaf forest
		2	Tropical or subtropical broadleaved deciduous forest—closed canopy	4	Deciduous broadleaf forest
		3	Temperate or subpolar broadleaved deciduous forest—closed canopy		
		29	Tropical or subtropical broadleaved evergreen forest—open canopy		
2	Needleleaf tree	4	Temperate or subpolar needleleaved evergreen forest—closed canopy	1	Evergreen needleleaf forest
		5	Temperate or subpolar needleleaved evergreen forest—open canopy	3	Deciduous needleleaf forest
		20	Subpolar needleleaved evergreen forest open canopy—lichen understory		
3	C3 grass	13	Temperate or subpolar grassland	10	Grasslands
		27	Wetlands	11	Permanent wetlands
		28	Herbaceous wetlands		
4	C4 plants	14	Temperate or subpolar grassland with a sparse tree layer (latitude < 40°N)	8	Woody savannas (latitude < 40°N)
		15	Temperate or subpolar grassland with a sparse shrub layer (latitude < 40°N)	9	Savannas (latitude < 40°N)
5	Shrubs	9	Temperate or subpolar broadleaved evergreen shrubland—closed canopy	6	Closed shrubland
		10	Temperate or subpolar broadleaved evergreen shrubland—closed canopy	7	Open shrubland
		11	Temperate or subpolar needleleaved evergreen shrubland—open canopy	8	Woody savannas (latitude ≥ 40°N)
		12	Temperate or subpolar mixed broadleaved and needleleaved dwarf shrubland—open canopy	9	Savannas (latitude ≥ 40°N)
		14	Temperate or subpolar grassland with a sparse tree layer (latitude ≥ 40°N)		
		15	Temperate or subpolar grassland with a sparse shrub layer (latitude ≥ 40°N)		
6	Tundra shrubs	16	Polar grassland with a sparse shrub layer		
		17	Polar grassland with a sparse shrub layer		
7	Barelands	21	Unconsolidated material sparse vegetation (old burnt or other disturbance)	13	Urban and built up
		22	Urban and built up	16	Barren or sparsely vegetated
		23	Consolidated rock sparse vegetation		
		25	Burnt area (recent burnt area)		
8	Crop	18	Cropland	12	Croplands
		19	Cropland and shrubland/woodland	14	Crop/natural vegetation mosaic
9	Mixed forest	6	Temperate or subpolar needleleaved mixed forest—closed canopy	5	Mixed forest
		7	Temperate or subpolar mixed broadleaved or needleleaved forest—closed canopy		
		8	Temperate or subpolar mixed broadleaved or needleleaved forest—open canopy		
10	Snow and ice	26	Snow and ice	15	Snow and ice
11	Water	24	Water	17	Water

3. Vegetation Initial Conditions

3.1. Experimental Design for Initial Vegetation Condition

Since the ecosystem model takes a long time to spin-up, it is necessary to obtain an equilibrium/quasi-equilibrium solution first for a specific DVM as its initial conditions for long-term simulations. Under a specified climate forcing, it normally takes 50–1000 years' simulation to reach equilibrium conditions [e.g., *Bonan and Levis*, 2006; *Zeng et al.*, 2008]. Since our goal is only to create initial conditions for the SSiB4/TRIFFID decadal simulations, rather than requiring hundreds to thousands of years of simulation to obtain an equilibrium solution, we find that a quasi-equilibrium solution, which only needs a 100 year simulation, is suitable for the SSiB4/TRIFFID decadal simulation without severe spin-up; the solution is also consistent to the current vegetation distribution.

To start the run for the quasi-equilibrium solution, a preliminary initial condition is also needed. There are different ways to set initial conditions for each PFT, i.e., its fractional coverage and LAI, for the quasi-equilibrium run. In some DVM models, the fraction of each PFT is set to zero in initialization for equilibrium runs; in some other models, equal fractional coverage for each PFT is assigned initially. After several tests, we found that using a SSiB vegetation table and a SSiB vegetation map, which are based on ground survey and satellite-derived information [*Dorman and Sellers*, 1989; *Xue et al.*, 1991, 1996,, 2004], is proper for the initial vegetation conditions for the quasi-equilibrium runs. Because of the uncertainty in a high-resolution satellite-derived vegetation map (~5 km), a dominant vegetation type is selected first for every 1° model grid box; i.e., in each grid point, only one vegetation type is initially selected; the fractions for other vegetation types are set to zero. The climate forcing as described in section 2.3.1 is used to drive SSiB4/TRIFFID for the quasi-
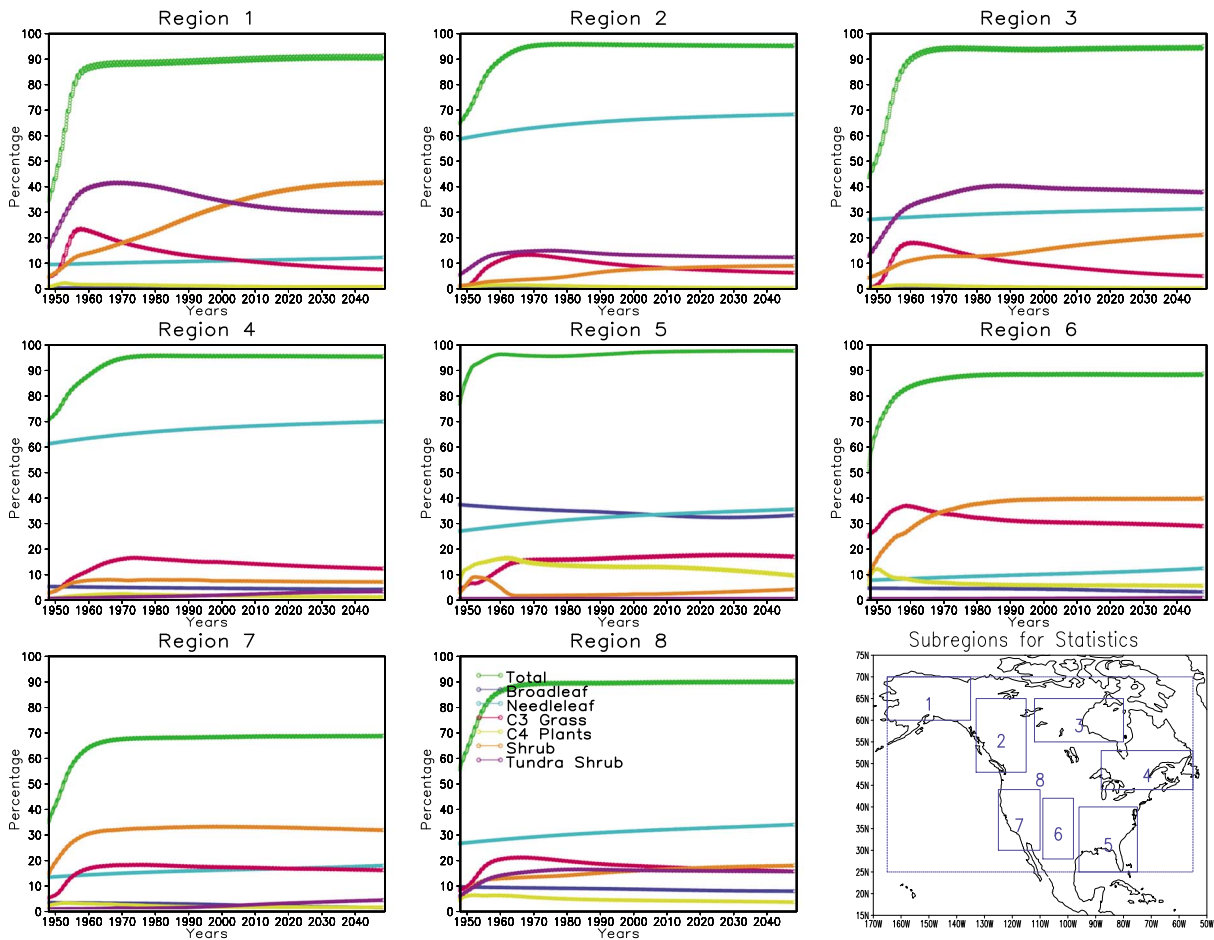
Figure 1. Temporal evolution of PFTs' fractional cover in the quasi-equilibrium simulation. The region areas are defined in the bottom right panel. The results are obtained after model improvements as discussed in section 3.2.

equilibrium run. The quasi-equilibrium run then produces the vegetation fractions for several PFTs, their LAIs, and other vegetation conditions in every grid point. In the quasi-equilibrium run, the 1948 atmospheric CO_2 concentration is used in the simulation. Otherwise, if we apply the initial vegetation conditions from the quasi-equilibrium run for the run with realistic meteorological forcing starting in 1948, which will be discussed in the next section, a dramatic LAI adjustment will occur because our model is a carbon balance model.

To better evaluate the temporal evolution of PFT fractions during the quasi-equilibrium runs, we divide the NA continent into eight regions as shown in Figure 1. Region 8 represents the entire North American continent. As shown in the figure, during the early time period of model integration, most vegetation fractions experience dramatic adjustments and then gradually approach quasi-equilibrium with time. We define that the quasi-equilibrium status occurs when the yearly changing ratio of vegetation fraction is less than 2% for the last 10 years of the equilibrium simulation. Our study indicates that for our model, a 100 year simulation is sufficient to reach quasi-equilibrium conditions if a few key parameters are properly selected. It should be pointed out that vegetation quasi-equilibrium state depends on spatial scales. When the averaged PFT fractions reach quasi-equilibrium over a region, some individual grid points within the region may still not reach quasi-equilibrium conditions. In this paper, the eight large regions are our main focus. Among the four northern regions, shrubs and tundra shrubs are dominant in Alaska; boreal forest dominates in Regions 2 and 4; and tundra shrubs, shrubs, and boreal forest are of mixed dominance in northern Canada. In the southeastern U.S., broadleaf trees and needleleaf trees are of mixed dominance and coexistent with C3 grasses. In the Midwest U.S., shrubs and C3 grasses are dominant, and in the western U.S. shrubs are the dominant type and are mixed with grasses and needle leaf trees. Such distribution is
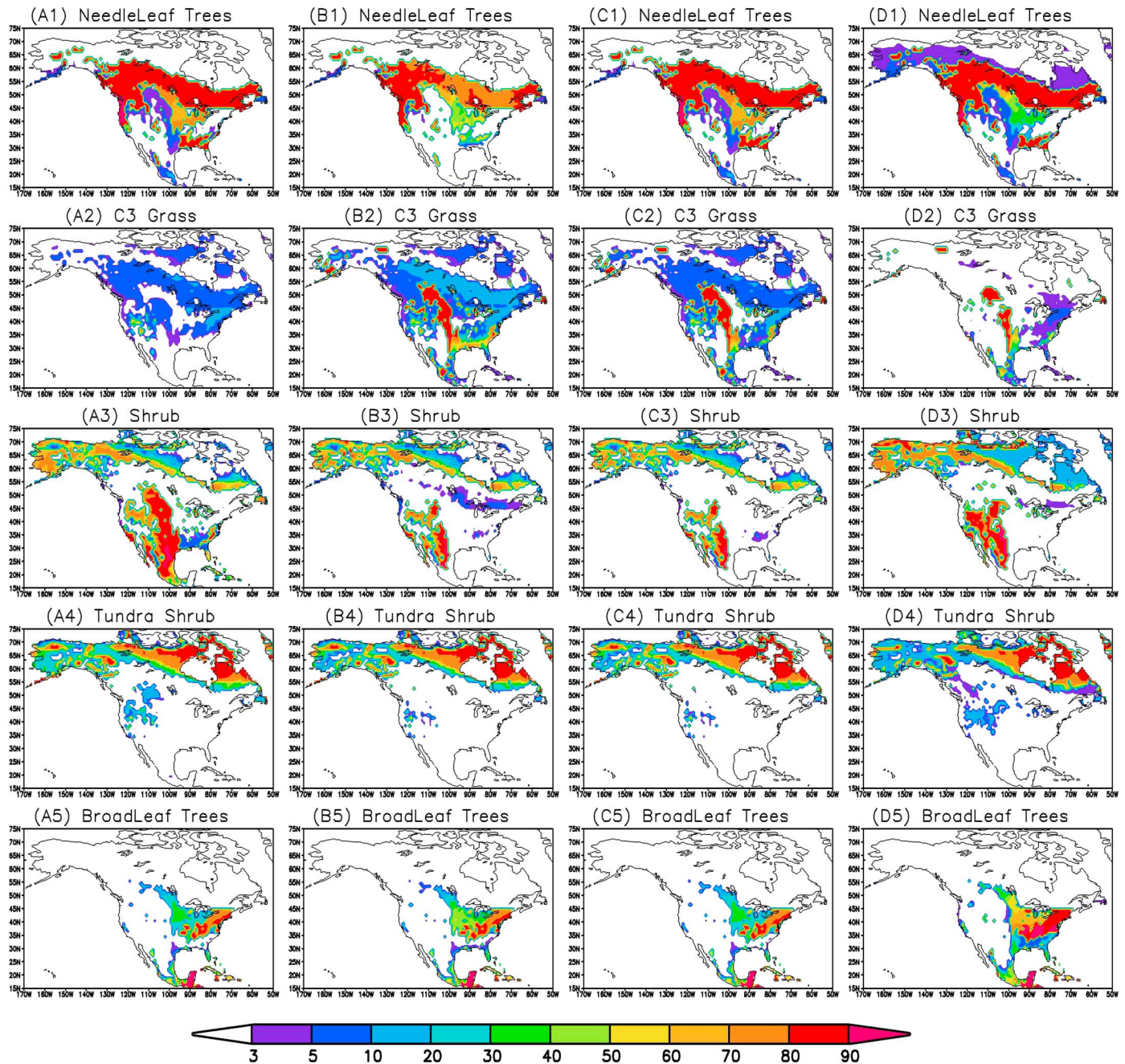
Figure 2. Five PFTs' fraction for the last 10 year average under equilibrium conditions, means under equilibrium conditions: (a1–a5) based on original TRIFFID setting; (b1–b5) changing the LV equation coefficients; (c1–c5) changing optimum temperature of photosynthesis of needleleaf trees; and (d1–d5) effect of leaf drop temperatures.

generally consistent with the published vegetation distribution [e.g., *DeFries and Townshend*, 1994; *Fennessy and Xue*, 1997; *MacDonald*, 2002; *Woodward et al.*, 2004].

3.2. Important Factors Affecting Quasi-equilibrium Status

Since the quasi-equilibrium run uses climatological forcing and simulation with real 1948–2008 climate forcing will not dramatically change the PFT spatial distributions from the quasi-equilibrium run (see next section), it should be expected that the general distribution with the climate forcing should be close to current vegetation distribution. In this section on the quasi-equilibrium run, we only discuss very obvious

Table 2a. Original Intraspecies Competition Relationships[a]

	i = 1 Broadleaf Trees	i = 2 Needleleaf Trees	i = 3 Shrubs	i = 4 Tundra Shrubs	i = 5 C3 Type Grass	i = 6 C4 Type Plants
j = 1 Broadleaf trees		*	1	1	1	1
j = 2 Needleleaf trees	*		1	1	1	1
j = 3 Shrubs	0	0		*	1	1
j = 4 Tundra shrubs	0	0	*		1	1
j = 5 C3 type grass	0	0	0	0		*
j = 6 C4 type plants	0	0	0	0	*	

[a]Note: Numbers i = 1–6 represent PFTs: broad leaf trees, needleleaf trees, C3 type grass, C4 type plants, shrub, and tundra shrubs, respectively. A value of 0 implies that PFT i dominates PFT j. A value of 1 implies that PFT j dominates PFT i. Asterisk indicates that two PFTs could coexist.

deficiencies in vegetation spatial patterns, such as whether there are grasslands in central U.S. For those features, the current knowledge of NA biogeography and vegetation mapping products provides a reasonable reference [e.g., *Fennessy and Xue*, 1997; *Ramankutty and Foley*, 1999; *MacDonald*, 2002]. The more detailed quantitative comparison with satellite-derived products will be presented in section 4, which presents the results using 1949–2008 meteorological forcing.

It should be pointed out that the quasi-equilibrium runs produce potential vegetation distributions, which sometimes are different from the current real situations over some areas as observed in satellite-derived products due to anthropogenic effects, such as the large areas in parts of NA with crops [*Ramankutty and Foley*, 1999]. There are no crops in TRIFFID.

Abiotic factors (e.g., soil texture), or climate-induced factors, as well as biotic factors affect PFT distribution and should be included in the DVM [*Pimentel et al.*, 2005]. The uncertainties induced by climate and model parameters can greatly influence the DVM-produced vegetation distribution. Using the Lund-Potsdam-Jena DVM, *Jiang et al.* [2012] found that parameters that control plant carbon uptake and light-use efficiency have predominant influence on the vegetation distribution of both woody and herbaceous PFTs; the relative importance of different parameters depends on the temporal and spatial scales under consideration and is also influenced by climate inputs. We have conducted a large number of experiments to test the effects of some important parameterizations/parameters that enable us to obtain quasi-equilibrium vegetation condition and produce a reasonable vegetation distribution, which should be generally consistent with the current dominant vegetation distribution. A few important factors play crucial roles in obtaining proper quasi-equilibrium conditions and are reported here. The results shown in Figure 1 were obtained after the improvement in the parameterizations/parameter setting.

3.2.1. Vegetation Competition Coefficients

Due to the difficulty in distinction between grasses and shrubs, some DVMs simply do not include shrubs in their models [*Zeng et al.*, 2008]. In order to properly produce shrub-dominated vegetation, a shrub submodule was designed in the Community Land Model; it includes appropriate parameters for shrubs and allows shrub growth only over areas that are not occupied by trees or grasses [*Zeng et al.*, 2008].

The PFT competition in TRIFFID is based on Lotka-Volterra (LV) equations, which describe the population dynamics of species competing for some common resource [*Silvertown*, 1987; *Cox et al.*, 2001; *Hughes et al.*, 2004]. The LV equations, however, sometimes lead to unrealistic outcomes. For instance, their equilibrium solutions prohibit the coexistence of PFTs in the absence of appreciable disturbance and temporal environmental variability [*Arora and Boer*, 2006]. In the SSiB4/TRIFFID, we allow the coexistence of different PFTs (Figure 1). However, these results are obtained after some adjustments to the environmental constraints in the model, such as wilting points and optimal photosynthetic canopy temperature. For example, it was found that with the original LV equation coefficients (Table 2a), shrubs completely took over grasses in some areas as shown in Figure 2a. The C3 grassland in the central U.S. was taken over by shrubs and almost disappeared completely. Based on current vegetation mapping and climate-vegetation biomes [e.g., *Ramankutty and Foley*, 1999; *MacDonald*, 2002], we understand such distributions are unrealistic. In the original TRIFFID, a (tree-shrub-grass) hierarchy was introduced for the PFT competition (i.e., shrubs dominate grasses, and trees dominate both grasses and shrubs) as shown in Table 2a, in which dominant types "i" limit the expansion of other types "j" ($c_{ji} = 1$) but not vice versa ($c_{ij} = 0$). However, this simplistic competitive hierarchy ignores

Table 2b. Modified Intraspecies Competition Relationships[a]

	$i = 1$ Broadleaf Trees	$i = 2$ Needleleaf Trees	$i = 3$ C3 Type Grass	$i = 4$ C4 Type Plants	$i = 5$ Shrubs	$i = 6$ Tundra Shrubs
$j = 1$ Broadleaf trees		*	1	1	1	1
$j = 2$ Needleleaf trees	*		1	1	1	1
$j = 3$ C3 type grass	0	0		*	*	*
$j = 4$ C4 type plants	0	0	*		*	*
$j = 5$ Shrubs	0	0	*	*		*
$j = 6$ Tundra shrubs	0	0	*	*	*	

[a]Note: Numbers $i = 1$–6 represent PFTs: broad leaf trees, needleleaf trees, C3 type grass, C4 type plants, shrub, and tundra shrubs, respectively. A value of 0 implies that PFT i dominates PFT j. A value of 1 implies PFT j dominates PFT i. Asterisk indicates that two PFTs could coexist.

factors such as importance of grass aleopathy on tree seedlings, root competition by established grasses precluding tree or shrub seedlings in arid grassland sites, or competitive advantages provided to grasses by sprouting or rapid maturation and seed set in fire-prone sites or heavily grazed systems [e.g., *Fales and Wakefield*, 1981; *Kolb*, 1988; *Higgins et al.*, 2000; *Fuhlendorf et al.*, 2008]. To overcome the problem of shrubs or trees simply overtaking grasses in all cases, we modified the order of competition as shown in Table 2b, which shows tree-grass-shrub dominance hierarchy. The C3 grasses and C4 are moved to $i = 3$ and $i = 4$, respectively. Meanwhile, we still allow shrubs and grasses to cocompete with competition coefficients dependent on their relative heights (see Table 2b). With this change, the model is able to produce the grasslands in the central U.S. as shown in Figure 2b. Although this change still seems unable to reproduce the full scope of grasslands, particularly in the western central plains, it is nevertheless a large improvement compared with Figure 2a.

3.2.2. Photosynthesis Optimum Temperature

Although grasslands in the central U.S. are present in Figure 2b, the figures also show a high proportion of grasses in the southeast U.S., which seems inconsistent with current conditions. According to the GLC2000 satellite data [*Latifovic et al.*, 2002], needleleaf and other trees cover a large percentage of the land in this area. However, the GLC2000 product also indicates a small swath of C3 grassland in the same area of the southeastern coastal region. We address this through scrutiny of photosynthesis.

Temperature is one of the principle factors having large effects on physiological activity at all spatial and temporal scales and is prominent among the major ecological variables that control plant distribution and productivity. Photosynthesis for all plants is strongly affected by temperature and shows an optimum temperature that roughly corresponds to the middle of the nonharmful (for photosynthesis) temperature range [e.g., *Berry and Bjorkman*, 1980; *Sage and Kubien*, 2007; *Taiz and Zeiger*, 2010]. The values for photosynthetic processes, including photosynthesis optimum temperature (POT), in SSiB4/TRIFFID are based on the SSiB vegetation parameter tables (see section 3.1), in which the C3 grasses' POT is closer to the annual mean temperature (290 K) in this area than that of needleleaf trees, which is relatively low. Although this SSiB POT parameter setting does not cause an obvious problem in simulation with specified PFTs, under fully coupled mode, it generates an unrealistic PFT distribution, indicating that the two-way coupling imposes a stricter constraint on model parameter settings. After several sensitivity tests and analyses, we determined that this was the cause for the C3 grasses taking over needleleaf trees in that area. By trial and error, we raised the needleleaf POT to 290 K, which is the annual mean surface temperature over that area (it was 288 K in the original SSiB table). Figure 2c shows that this approach solved the problem in the southeastern U.S. coastal areas and meanwhile had no large impact on other areas' grassland distribution. Compared with the original setting, the needleleaf trees also extend to the south a little bit in the central U.S. This is crop area in today's satellite-derived map. Most crop area in the central U.S. could potentially grow as prairie and the needleleaf trees that existed there some 200 years ago [*Carroll et al.*, 2002; *Middleton*, 2008].

Table 3. Settings of Temperatures Below Which Leaves Are Dropped (K)

Experiments	Broadleaf Trees	Needleleaf Trees	C3 Type Grass	C4 Type Plants	Shrubs	Tundra Shrubs
Equilibrium run	284.15	265.15	268.15	268.15	273.15	268.15
Original TOFF run	273.15	243.15	258.15	258.15	243.15	N/A
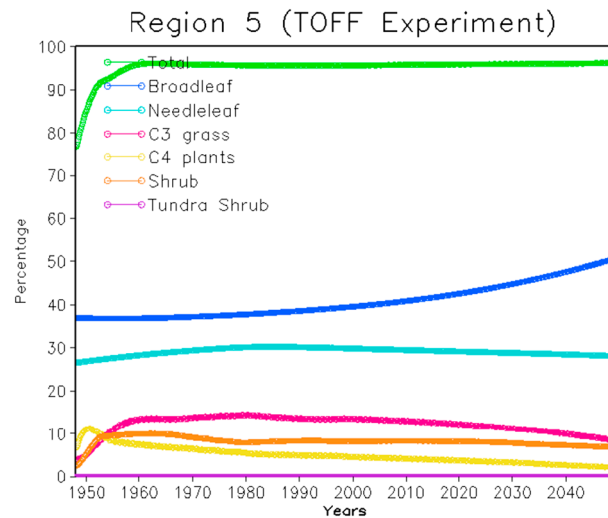
Figure 3. PFT fraction evolution for Region 5 after changing TOFF.

3.2.3. Leaf Drop Threshold Temperatures

In addition to the two above factors, the setting of leaf drop threshold temperatures (TOFF) is very critical for vegetation phenology and affects the PFT spatial distribution. In TRIFFID, leaf mortality rates are assumed to be a function of temperature as the leaf temperature drops below a threshold value, TOFF. When the environmental temperature is higher than TOFF, the leaf mortality rate in TRIFFID is set to minimum value. The original TOFF in TRIFFID was quite low (Table 3) such that there was no significant seasonal variation because the environmental temperature was most likely higher than TOFF [*Murray-Tortarolo et al.*, 2013]. To produce proper seasonal and interannual variability, we have adjusted TOFF for each PFT (Table 3)

enlightened by the SSiB4/TRIFFID tests in several sites with different PFTs over the globe [*Xue et al.*, 2006]. Following that approach, the TOFFs were adjusted for this study. To demonstrate the TOFF effect, we made a quasi-equilibrium run with the original TRIFFID TOFF (see Table 3). Since there was no tundra shrub in the original TRIFFID, we use the same TOFF of the shrubs for tundra. With the original TOFF setting, which is much lower than the SSiB4/TRIFFID setting, shrubs and tundra shrubs grow more at high latitudes and extend further to the south. The model is unable to produce a reasonable spatial distribution of C3 grasslands (Figure 2d) because the shrubs and tundra extend much too far to the south and displace C3 grasslands.

The settings of TOFF not only affect the vegetation distribution pattern but also affect the simulation of vegetation equilibrium status for some plant taxa. For example, as shown in Figure 3, for Region 5 the needleleaf trees accelerate their growth with time and gradually overtake other vegetation types. The vegetation does not reach equilibrium status even after 100 years' simulation.

4. Simulation Results Using the 1948–2008 Meteorological Forcing

4.1. Simulated and Satellite-Derived Vegetation Distribution

We used the quasi-equilibrium outputs as discussed in section 3.1 as initial vegetation conditions, which include each PFT's fraction, LAI, etc. at every grid point to integrate the model using the meteorological forcing from 1948 to 2008 (section 2.3.1). *Anav et al.* [2013] have shown that adequate vegetation fraction is more important in "controlling the distribution and value of LAI than the climatic variables." They also found that because of this, in their model intercomparison study, the models with prescribed vegetation distribution performed better than those DVMs which dynamically simulate the vegetation fraction distribution but with unrealistic distribution. Therefore, we assess the model vegetation fraction products first by comparing the simulated dominant vegetation type distribution based on the averaged vegetation fractional coverage from 1998 to 2008 (Figure 4c) with satellite analyses, which only provide comparable products during this time period. The distribution of vegetation types from the land cover database of GLC2000 [*Latifovic et al.*, 2002] is shown in Figure 4a, and the dominant vegetation type based on the MODIS IGBP vegetation fraction from 2001 to 2010 is shown in Figure 4b [*Friedl et al.*, 2010]. Please note that their vegetation types have been converted to the SSiB4/TRIFFID types (Table 1).

For both the simulated and satellite-observed vegetation distributions, needleleaf trees dominate in the northern midlatitudes of the NA continent. The spatial distribution of boreal forest band there shows a slight northwest-southeast direction. However, the MODIS IGBP product shows a much narrower boreal forest band in the midlatitudes compared with the other two products and presents larger mixed forest and shrub bands there. Meanwhile, GLC2000 and SSiB4/TRIFFID have needleleaf trees dominant in the southeast U.S. but almost negligible in the MODIS IGBP map, which identifies the area as mixed forests. Table 4
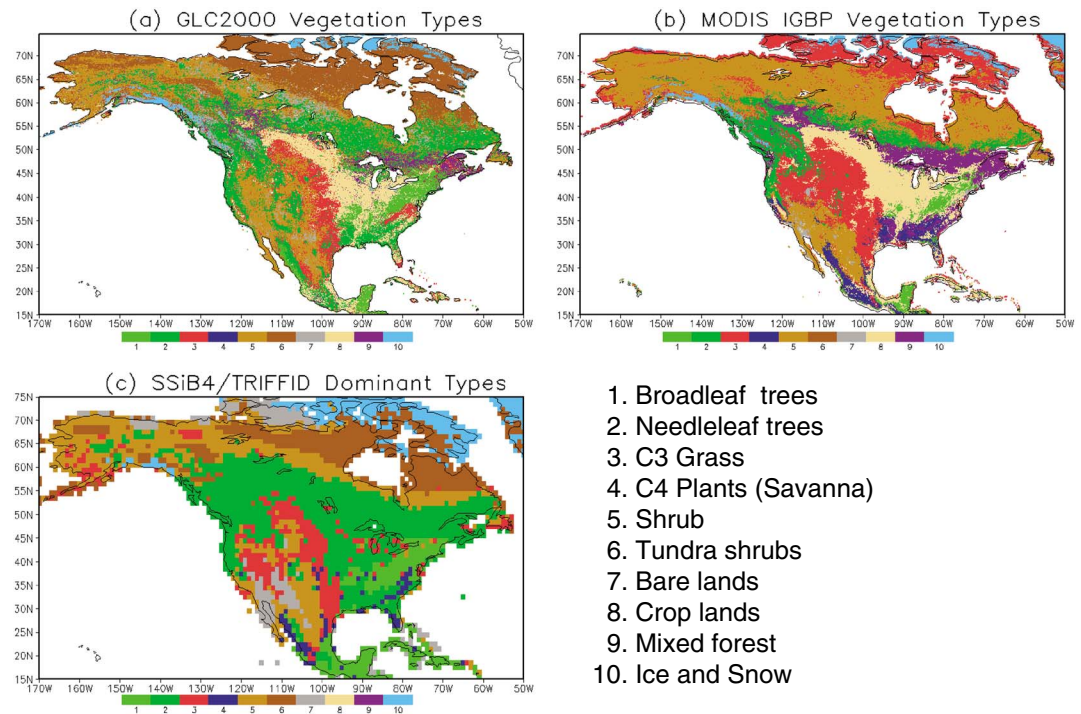
Figure 4. Comparison of simulated and satellite-derived dominant PFTs. (a) GLC2000; (b) MODIS IGB vegetation types based on averaged vegetation coverage for 2001–2010; and (c) SSiB4 simulation based on averaged vegetation coverage for 1998–2008.

shows the PFT fractional coverage for each region. For Region 5 (the southeast U.S.), SSiB4/TRIFFID produces 35.5% broadleaf trees and 36.2% needleleaf trees, which actually are mixed forests. In central NA, west of the Great Lakes, the model produces a larger area of needleleaf trees, but the area is currently covered by crops in satellite products, indicating the effects of human activities. The MODIS IGBP products do not distinguish shrubs and tundra. The shrubs and tundra shrubs in GLC2000 and SSiB4/TRIFFID are quite consistent. Between tundra and boreal forest, SSiB4/TRIFFID shows a transition zone of shrubs, consistent with MODIS in that area but different from the GLC2000 map in Canada, which shows a sharper needleleaf trees/tundra transition. The MODIS and SSiB4/TRIFFID portrayal appears more consistent with current ecological conditions in terms of a gradual transition from forest to tundra [*Ecological Stratification Working Group*, 1996]. Over Alaska, the SSiB4/TRIFFID-simulated distribution and GLC2000 map have very similar spatial patterns of tundra shrubs, shrubs, and needleleaf trees. Over the eastern U.S., the simulated broadleaf trees well reproduced the satellite-derived distribution. By and large, over these areas, simulated results are relatively close to GLC2000.

In the southwestern and central U.S., short plants are dominant. Despite the general agreement on the distribution patterns (i.e., grassland in the central U.S. and shrubs over the lower elevation southwestern U.S.),

Table 4. PFT Fractional Coverage (%) Averaged From 1998–2008 and From the Equilibrium Runs[a]

PFTs/Area No.	Broadleaf Trees	Needleleaf Trees	C3 Grass	C4 Plants	Shrubs	Tundra Shrubs	Total Coverage	FASIR
1		13.4 (11.9)	1.6 (1.9)		**47.3** (**46.0**)	27.0 (31.1)	89.3 (90.9)	87.4
2		**67.7** (67.4)	5.7 (5.5)		9.8 (9.6)	10.9 (12.8)	94.2 (95.4)	92.7
3		31.5 (31.1)	5.1 (4.8)		24.2 (20.5)	**31.9** (38.1)	92.7 (94.5)	74.2
4	3.0 (3.7)	**69.9** (69.3)	7.9 (8.0)		10.0 (10.1)	2.8 (3.8)	96.6 (94.9)	96.6
5	**35.5** (33.6)	**36.2** (35.1)	13.2 (15.7)	2.1 (3.2)	8.1 (8.4)		95.2 (96.0)	97.3
6	0.5 (0.6)	11.0 (11.3)	19.8 (22.6)	1.6 (1.7)	**40.4** (48.1)	0.2 (0.8)	73.4 (85.0)	54.0
7	0.5 (0.6)	12.5 (11.7)	16.6 (11.3)	0.2 (0.2)	**22.5** (30.2)	0.8 (2.3)	53.0 (56.4)	44.7
8	6.8 (7.0)	**34.0** (32.9)	10.9 (11.2)	0.7 (0.8)	21.1 (21.6)	13.3 (15.7)	86.7 (89.1)	77.8

[a]Note: (1) Equilibrium run values are listed in parentheses. (2) FASIR only provides the total vegetation coverage. (3) The values for dominant types are in bold.
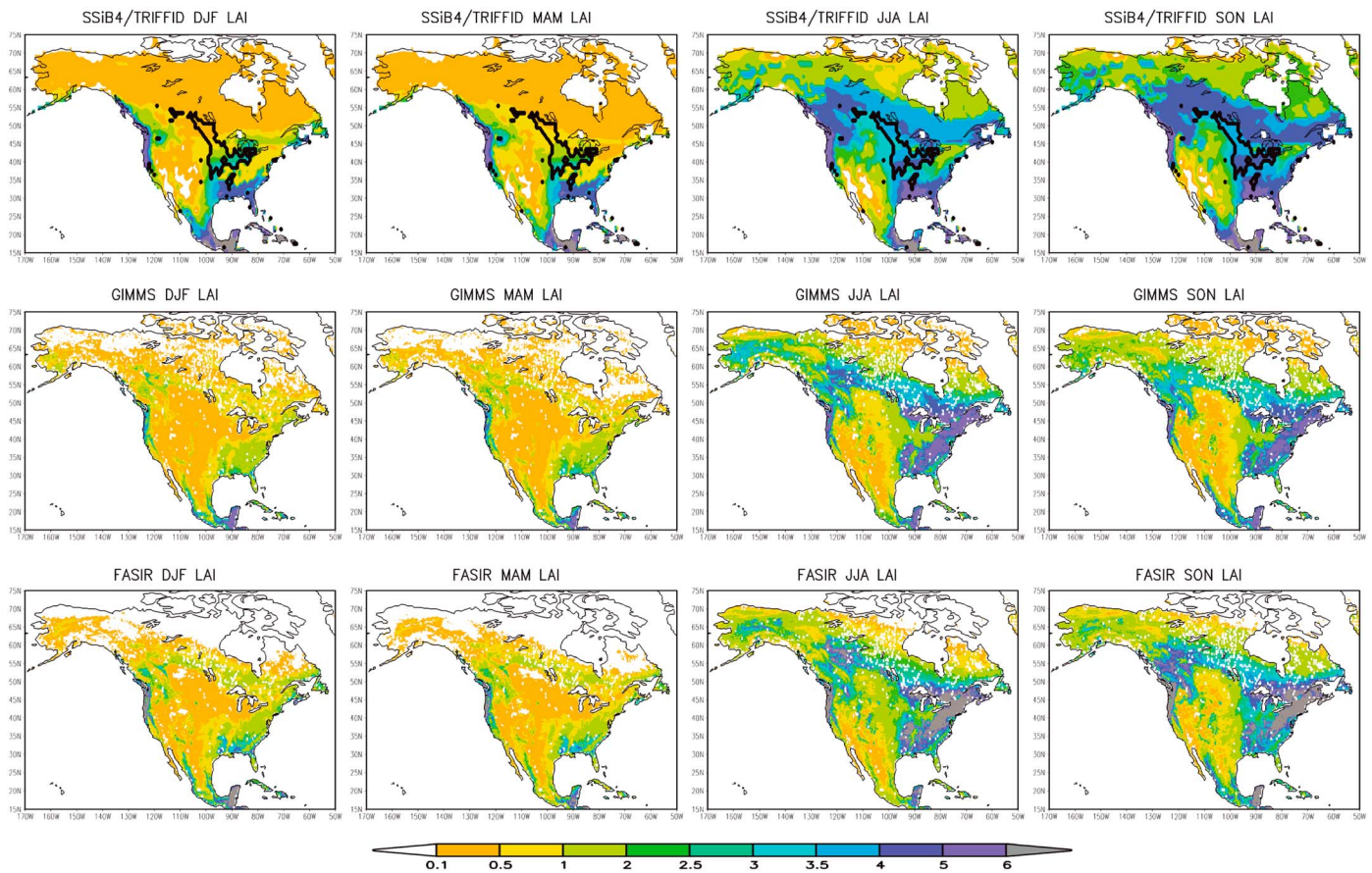
Figure 5. Comparison of simulated and satellite-derived LAIs (the solid enclosed crop curve in simulated LAI figures is based on initial satellite crop).

there are appreciable differences between GLC2000, MODIS IGBP, and simulation, indicating the difficulty in identifying short plant land cover (grasslands versus shrubs) or bare ground portions over those regions. The MODIS IGAP and SSiB4/TRIFFID map have larger grassland coverage in the Great Basin region than the GLC2000 product. Meanwhile, the SSiB4/TRIFFID model simulates bare ground desert in large parts of the southern southwestern U.S., where shrubs are identified as dominant in satellite products. The difficulty in reproducing the dominant types over southwestern to central NA may suggest the existence of other mechanisms unaccounted for in the simulation. *D'Odorico et al.* [2007] suggest that based on their data, "the tendency of the system to exhibit two (alternative) stable states becomes stronger in the more arid regions. Thus, at the desert margins, vegetation is more likely to be prone to discontinuous and abrupt state changes." Although the general distribution of lower elevation short vegetation/bare ground is captured well in the southwestern U.S., adequate simulation of the specific arid lands groundcover conditions there (grassland, shrub, bare ground) remains a great challenge. The SSiB4/TRIFFID has difficulty simulating C4 plants over North America when we compare the SSiB4/TRIFFID-simulated C4 plants with the MODIS savanna lands (Figure 4) and the C4 plan distribution discussed in *Still et al.* [2003]. GLC2000 has no C4 plants for comparison. The model seems to be capable of producing C4 in other parts of the world (not shown) but not in NA. Our approach on initial vegetation condition may also contribute to this deficiency. Savannas are known to depend on climatic variability, and our forcing for the equilibrium run for the initial vegetation is a climate forcing without interannual variability, which may underestimate the C4 distribution. The cause for this deficiency over NA is still under investigation.

The statistics of the fractional coverage over the eight regions averaged from 1998–2008 are summarized in Table 4. For comparison, the results from the quasi-equilibrium runs are also listed in parentheses. In most areas, the fractional coverage is still very close to the quasi-equilibrium run, indicating that our quasi-equilibrium run's results are generally stable. The MODIS data provide the fractional coverage for a few PFTs, but it is normally

Table 5. Spatial LAI Correlation Between TRIFFID and Satellites (165°W–55°W, 25°N–70°N) (1982–1998 Average)

Names	Calculation	DJF	MAM	JJA	SON	Year
TRIFFID and GIMMS	Correlation	0.61	0.67	0.58	0.66	0.59
TRIFFID and FASIR	Correlation	0.67	0.71	0.59	0.65	0.67
GIMMS and FASIR	Correlation	0.84	0.87	0.90	0.92	0.91
TRIFFID	Averages	1.12	1.07	2.66	2.89	1.94
GIMMS		0.66	0.71	2.21	2.04	1.44
FASIR		0.79	0.72	2.27	2.39	1.55

always close to either 1 or 0. Better satellite products for fractional vegetation coverage are necessary for further model validation. For a reference, we list FASIR's total vegetation coverage percentage for these regions for comparison. Except for Regions 3 and 6, the total vegetation covers with FASIR and with SSiB4/TRIFFID are quite close.

4.2. Spatiotemporal Variability of Vegetation LAI
4.2.1. Spatial Distributions of the Simulated and Satellite-Derived LAIs

In SSiB4/TRIFFID, LAI is calculated based on parameters describing the minimum and maximum LAIs for a given PFT specified in TRIFFID, carbon balance, and phenological processes, which depend on leaf temperature and soil moisture. Figure 5 shows the simulated and satellite-derived LAI spatial distributions in winter (DJF, December, January, February), spring (MAM, March, April, May), summer (JJA, June, July, August), and fall (SON, September, October, November) averaged from 1982 to 1998, a time period when both FASIR and GIMMS data exist. We have received the latest GIMMS LAI data [*Zhu et al.*, 2013], which extend to 2010. However, since this new LAI data set shows no relationship at all with climate variables but the old one shows a clear relationship, consistent with the GIMMS NDVI products [*Zeng et al.*, 2013], in this paper we still use the old GIMMS data set, which ends in 2002.

The FASIR and GIMMS satellite data products show similar spatial patterns: large LAI over boreal forest area, the eastern U.S., Central America, coastal areas in the northwest U.S., and southeast Canada with large seasonal variations (except tropical rainforests). FASIR JJA LAIs over boreal forests and over the eastern U.S. are larger than GIMMS'. In addition, despite the general agreements over Alaska and the western U.S., differences in some detailed structures in spatial distributions between these two data sets are apparent. For instance, GIMMS shows lower JJA LAI over the Sierra Nevada but higher JJA LAI over Alaska compared to that of FASIR. The SSiB4/TRIFFID simulation generally reproduces the major LAI spatial distribution patterns and temporal variation shown in the two satellite products. Table 5 shows the spatial correlations between SSiB4/TRIFFID and satellite products. *Murray-Tortarolo et al.* [2013] report the DVM comparison results for northern high latitudes, and the correlations/bias are much lower/higher than listed in Table 5. For instance, the correlation coefficients are around 0.6 to 0.7 in Table 5 and 0.21 for TRIFFID, which was the original version and was not coupled with SSiB, in *Murray-Tortarolo et al.* [2013]; the bias is about 1 over boreal forest in this study, much lower than 3–4 as reported in *Murray-Tortarolo et al.* [2013]. *Murray-Tortarolo et al.* [2013] speculate that the lesser number of PFTs in TRIFFID may cause the low correlation, but they are also concerned that more PFT numbers could lead to an increased uncertainty due to their parameterizations, while an insufficient number results in a misrepresentation of vegetation dynamics. This study shows that proper presentation of phenological processes and photosynthesis processes plays a crucial role in producing NA LAI seasonal spatial distribution. Whether increasing PFTs will further help the SSiB4/TRIFFID simulation needs further investigation.

It should be pointed out that although the SSiB4/TRIFFID shows that bare ground is dominant over part of the western U.S., which is different from satellite products (Figure 4), its LAI value and its seasonal variation are actually slightly higher than the satellite products. However, the SSiB4/TRIFFID simulated LAI values are lower than satellite products over the eastern U.S. in summer and over the boreal forest area in winter but higher in the southern U.S. in spring. The lower LAI in the northeastern U.S. is caused by the setting for POT for the broadleaf trees. In TRIFFID, the parameters for evergreen and deciduous trees are not separated. While the setting is good for the broadleaf trees over the Amazon and Central Africa, it is not adequate for the deciduous broadleaf trees in the northeastern U.S. Some other differences between the simulation and satellite products may be caused by human impact on land cover which is captured in the satellite products but not simulated by SSiB4/TRIFFID. For instance, many crops grow in the central U.S. (the thin solid line in
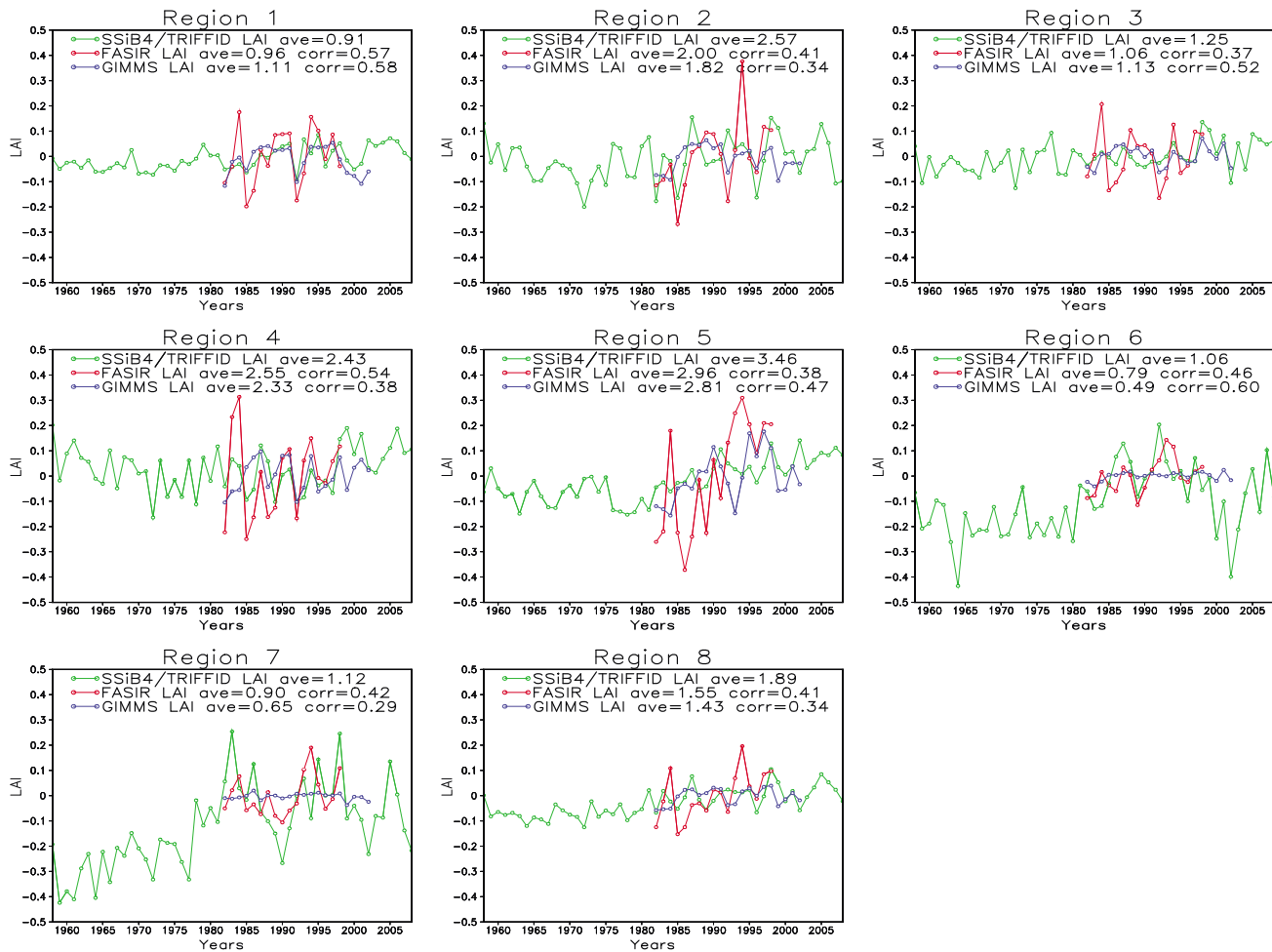
Figure 6. Simulated and satellite LAI temporal evolutions from 1958 to 2008.

Figure 5). The simulated LAI, based on SSiB4/TRIFFID simulated potential vegetation, i.e., needleleaf trees, is greater than that of observation.

4.2.2. Temporal Changes of the Simulated and Satellite-Derived LAIs

Figure 6 shows comparisons of the anomalies of annual mean LAI between the simulation and satellite products for the eight regions from 1958 to 2008. We take out the first 10 years' simulation and only show the results from 1960 to 2008 because we are not sure whether any trends during the first 10 years are still affected by the spin-up. The FASIR data show relatively large variances compared with GIMMS, which has been discussed in *Kang et al.* [2007]. The FASIR and GIMMS are derived from the same satellite products. The differences are mainly caused by different retrieval algorithms and atmospheric correction methods. The correlation coefficients of the simulated LAI with GIMMS LAI and FASIR LAI over these regions are listed in Table 6. The numbers of degrees of freedom in calculating the statistical significances in Tables 6 and 7 have been adjusted to take into account the autocorrelation in the time series data using the *Dawdy and Matalas* [1964] method. The correlation coefficients for the interannual variability from 1982 to 1998 (for FASIR) and 2002 (for GIMMS) ranged from 0.37 to 0.57 for FASIR and from 0.29 to 0.58 for GIMMS. The correlation coefficients with statistical significance at the $\alpha = 0.01, 0.05$ level of t test values are listed in bold and italics, respectively, in Table 7. Only in Regions 2 and 7 does the simulated LAI have no statistically significant relationship with either of the satellite products. It is interesting to notice that over the entire domain, the model results and satellite products have no significant relationship. We will discuss this issue in the next section.

Although there are no clear trends in PFT fractions, which confirm that our initial conditions are generally adequate, a few regions show clear LAI trends in past decades. It was reported that California and adjacent

Table 6. Temporal Correlations of Simulated and Satellite-Derived LAI

Area No.	Longitude (deg)	Latitude (deg)	1982–1998	
			GIMMS LAI	FASIR LAI
1	165W–135W	60N–70N	0.577***	0.567***
2	134W–115W	48N–65N	0.342	0.414**
3	112W–80W	55N–65N	0.524***	0.370
4	88W–55W	44N–53N	0.381	0.538***
5	95W–75W	25N–40N	0.474*	0.380
6	109W–100W	30N–42N	0.598***	0.459*
7	125W–110W	30N–40N	0.295	0.425*
8	165W–55W	25N–70N	0.344	0.406*

*Results are statistically significant at 0.12 significance level.
**Results are statistically significant at 0.10 significance level.
***Results are statistically significant at 0.05 significance level.

regions experienced one of the most severe droughts during 1987–1992 [*Brumbaugh et al.*, 1994] and during the last decade [*MacDonald*, 2010]. The drought effects on vegetation can be clearly seen in Region 7. There was also a rapid increase in LAI approximately from 1960 to 1980, when no satellite data are available for comparison. However, 1960 to 1980 was a period of generally increasing precipitation and decreasing aridity as measured by the regional Palmer Severity Index [*MacDonald*, 2010]. This increase in moisture was coupled with warming [*MacDonald*, 2010], and this likely would have promoted enhanced vegetation growth and LAI. Furthermore, both the simulation and satellite observations identify LAI increase in Region 5, i.e., the southeastern U.S. starting from the 1980s. For the entire NA continent, the simulated LAI and the satellite observations all show an increasing trend approximately since 1970 (for simulation) and 1982 (for satellite) until the end of our simulation. This increasing trend likely results from the impacts of increasing CO_2 enrichment and climate change-related warming and regional increases in precipitation on plant growth and LAI [*Piao et al.*, 2006]. The discussion of detailed causes and mechanisms of these trends and large variations are beyond the scope of this paper.

## 5. Relationships Between Vegetation and Climate/Surface Condition

The discussion in section 4 shows that the SSiB4/TRIFFID-produced vegetation properties are generally consistent with the satellite products. These results were driven by meteorological forcing. Based on 85 in situ worldwide measurements, *Hawkins et al.* [2003] found that measures of energy, water, or water-energy balance explain the geographic pattern in species richness better than other climatic and nonclimatic variables. In this section, we assess the relationship between observed and simulated spatial and temporal variability of vegetation with climate and surface conditions. This paper has demonstrated the importance of climate on the model-simulated vegetation distribution. Therefore, it is important to evaluate whether this model produced a valid climate/vegetation relationship.

The statistical calculation for our analysis is conducted for every 1° grid box from 1948 to 2008 for SSiB4/TRIFFID and from 1982 to 1998 for the GIMMS and FASIR satellite products, a time when both sets of satellite data are available. The seasonal mean data were used in the statistical analyses. After investigating the correlations

Table 7. Temporal Correlations of Simulated LAI With Surface Temperature and Soil Moisture[a]

Area No.	1948–2008 ($\alpha = 0.05$)		1982–2002 (GIMMS) ($\alpha = 0.1$)		1982–1998 (FASIR) ($\alpha = 0.1$)	
	Temperature	Soil Wetness	Temperature	Soil Wetness	Temperature	Soil Wetness
1	*0.66*					
2	*0.67*		**0.49**			
3	*0.64*		**0.50**			
4	*0.71*				**0.51**	
5	*0.75*					
6		*0.57*				
7		*0.78*		**0.39**		**0.45**
8	*0 70*		**0.45**		*0 48*	

[a]Note: Only values with 0.05 or 0.1 statistical significance level are listed in italics and bold respectively.
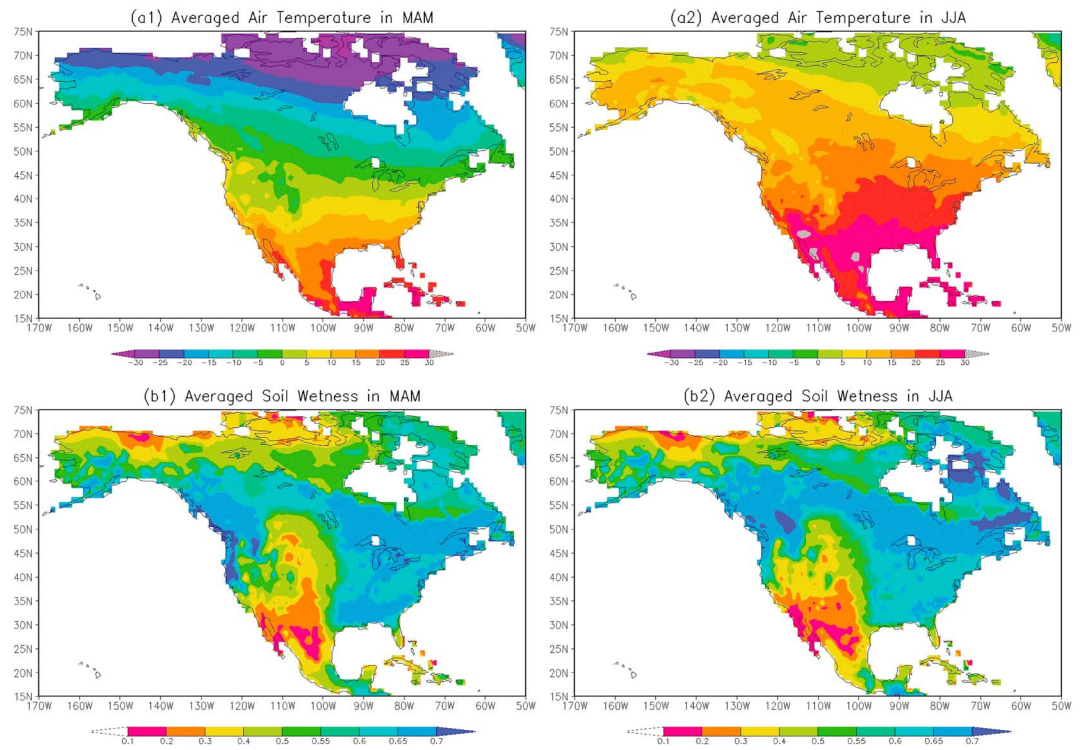
Figure 7. Averaged for MAM and JJA from 1998 to 2008: (a) observed air temperature (°C) and (b) simulated soil wetness.

of the simulated LAI, GIMMS, and FASIR LAIs with simulated soil wetness at the rooting zone, and observed precipitation and air temperature as presented in section 2.3 for different seasons, it is found that only MAM and JJA conditions show a significant relationship between LAI and environmental variables over large areas, consistent with the results for the NA region from a general circulation model study [*Xue et al.*, 2010].

The satellite products have a high positive correlation between LAI and spring air temperature (Figures 8t2 and 8t3) over northern middle to high latitudes of NA, except near the Arctic region, consistent with *Zeng et al.*'s [2013] results, which used the NDVI as the proxy for vegetation. High temperatures during the spring affect vegetation phenology and length of the growing season, which should contribute to this positive correlation. It is not surprising to see that the southern boundary of the high correlation area approximately follows the line with seasonal mean temperature at 5°C (Figure 7a1), which is coincident with the low-temperature stress factor of photosynthesis of the needleleaf trees, the dominant PFT at that location. The satellite products show many small discrete spots within these areas with zero correlation, reflecting a quality issue in these pixels. In general, the model simulation also produces a positive anomaly similar to the satellite products but with higher correlations than the satellite products. Meanwhile, the areas with positive correlation extend much to the north, close to the Arctic area, compared to the satellite products.

We conducted statistical analysis for LAI and spring precipitation, but that did not yield statistically significant correlations, which is consistent with *Zeng et al.*'s [2013] results. However, *Zeng et al.* [2013] found that positive correlations were the strongest and most spatially extensive at a lead of 1 month, and locally significant positive correlations could last up to a lead of 6 months. Since the hydrological variable that affects the vegetation growth most is soil moisture, and precipitation via soil moisture affects plants, we conducted a statistical analysis using model-simulated rooting zone soil wetness and LAI.

The area of high positive correlation with soil moisture (Figures 8w2 and 8w3) is mostly located in the semiarid southwestern U.S. and Mexico, where the soil wetness is lower than 0.3 (Figure 7b1) and covers grasslands, shrublands, and savannas. The positive correlation between soil wetness and satellite-derived NDVI in arid and semiarid landscapes has been detected in some studies [e.g., *Nemani et al.*, 2003; *Zribi et al.*, 2010]. The SSiB4/TRIFFID simulation also shows high positive correlations with soil moisture over shrubs and tundra areas near the Arctic Ocean and North Atlantic. But this correlation is not as strong in satellite
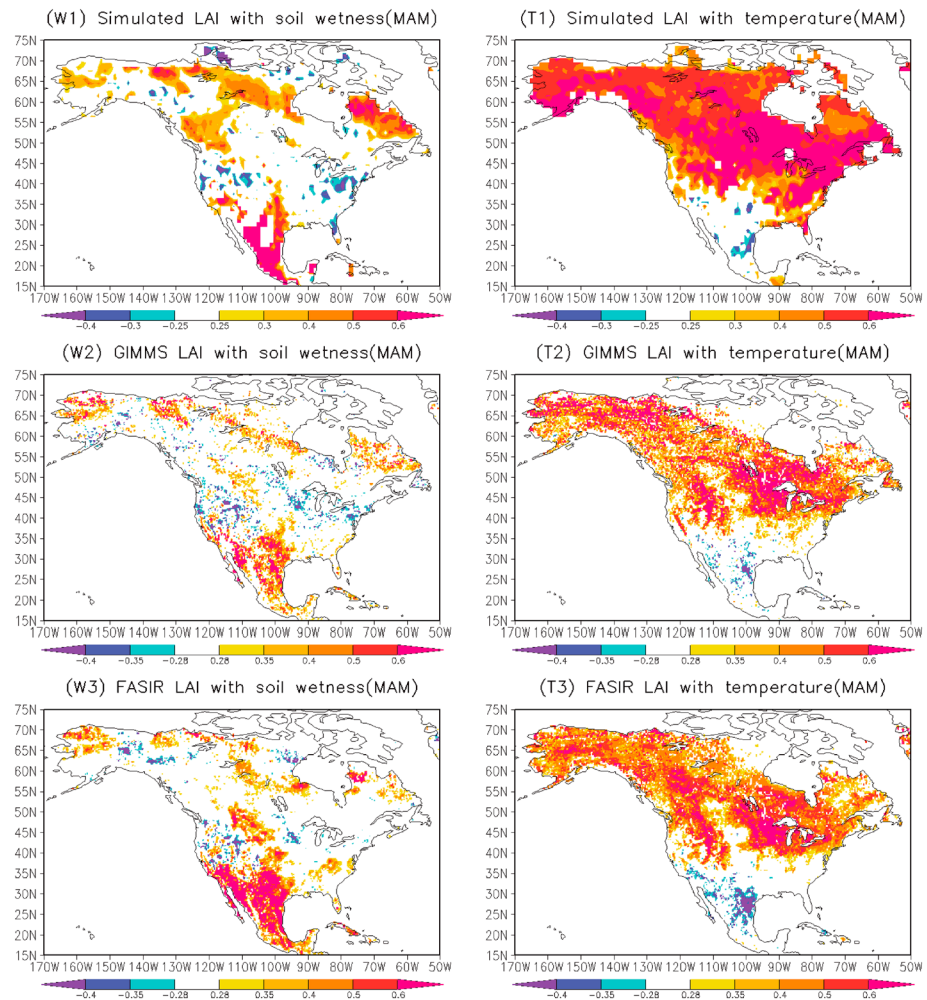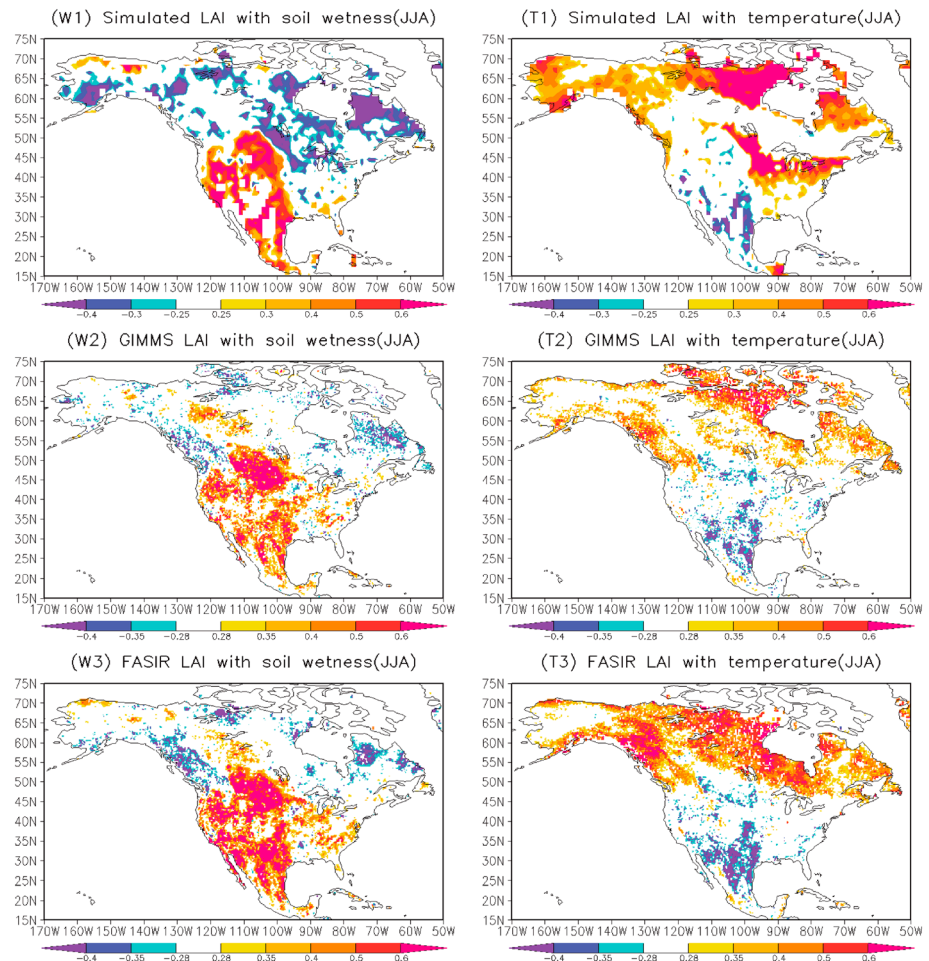
Figure 8. Correlation of simulated and satellite-derived MAM LAIs with simulated soil wetness and air temperature.

products. Moreover, there are discrepancies between the simulated and satellite-derived relationships over southwestern Canada: the SSiB4/TRIFFID results show a correlation with soil wetness, but it is not apparent in the satellite products. The temperatures over those areas are generally lower than 0° during this time period. Although liquid soil moisture still exists under frozen conditions [*Li et al.*, 2010] and shows some positive correlation (Figures 8w2, and 8w3), the model-simulated relationship between LAI and soil moisture may be exaggerated because in the SSiB version for this study, the frozen soil submodule is not included.

The strong coupling between vegetation and climate in spring over NA has been reported in other modeling and diagnostic studies. For example, *Xue et al.* [2010] have conducted a global and seasonal assessment of regions of the Earth with strong climate-BGP interactions. They identify that in the eastern and western U.S. and the Canadian boreal area the spring season exhibits a very strong interaction with vegetation conditions. A positive relationship between LAI and spring air temperature has also been reported based on observed climate data and NDVI, especially across the northern U.S. [e.g., *Notaro et al.*, 2006; *Wang et al.*, 2011].

During the summer (JJA), the areas with high correlation coefficients between LAI (Figure 5) and temperature (Figure 7a2) become smaller and move to the north in the satellite products and model simulation (Figure 9), consistent with temperature change. Meanwhile, the semiarid area over the southwest U.S. shows negative correlation; i.e., higher temperature in these dry lands (Figure 7a2) may have a negative effect on vegetation growth through its direct adverse impact on photosynthetic processes and growth, as well as through its interactions with soil moisture. The correlation between the JJA surface temperature and soil moisture in the southwest U.S. is around negative 0.5 (not shown). The correlation between LAI and soil wetness increases
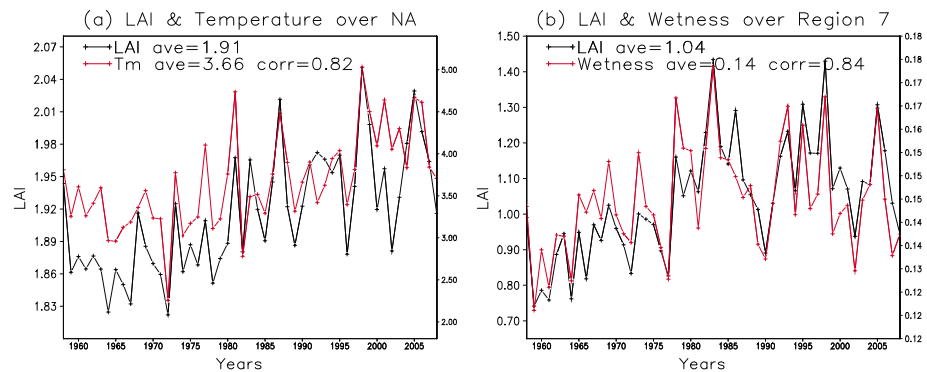
Figure 9. Correlation of simulated and satellite-derived JJA LAIs with simulated soil wetness and air temperature.

substantially, especially over the dry lands of the western U.S. (Figure 9). Some of these areas have correlations between LAI and soil wetness of more than 0.5, indicating vegetation's high demand for water during the summer season. It is very interesting to see that the spatial patterns of correlation between LAI and soil moisture are very similar to the ones for LAI and 1–3 month lead precipitation in both spring and summer, which suggest that precipitation seems to affect the vegetation through soil moisture memory, which is also influenced by temperatures and resulting evaporation rates. This relationship is also consistent with other modeling studies [e.g., *Asharaf and Ahrens*, 2013].

In recent studies on summer vegetation browning in NA, some speculated that it was due to increased drought stress, driven by rising summer temperature [*Angert et al.*, 2005], decreasing precipitation [*Zhang et al.*, 2010], or other climate drivers [*Wang et al.*, 2011]. These studies confirm the intuition that soil moisture availability does have strong effects on vegetation, with the strongest effects under the condition that the soil is very dry during a hot summer. All these results are consistent with the relationships discussed in this study.

Table 7 lists the correlation coefficients over the eight study regions to more clearly summarize the relationships that we discussed above. The correlation coefficients between simulated LAI and air temperature for Regions 1–5 and the entire continent are statistically significant at $\alpha = 0.05$ level (t test), while the correlations between simulated LAI and soil wetness are statistically significant over Regions 6 and 7, which cover dry lands. The relationship between satellite-derived LAI and climate seems not as strong as shown in the simulation. Only LAI in Regions 2, 3, and 5 shows statistically significant correlations with temperature and only LAI in Region 7 shows a significant relationship with soil moisture. The surface temperature has a warming trend

Figure 10. Time evolution of simulated (a) LAI and surface temperature (°C) over North America and (b) LAI and soil wetness over Region 7.

after 1970 (Figure 10a). The LAI follows this trend very well (Figures 6 and 10a). The correlation coefficient, 0.70, is quite high for simulated LAI over NA but <0.5 for satellite-derived products, which may be a partial reason why the simulated and satellite LAIs have low correlation over NA (Table 6). The reasons for the discrepancies between the strength of correlations in the simulation compared to the satellite products are unclear. Whether this is because the model results are too dependent on the selected climatic drivers, which obscures relations with other factors, and/or satellite products having shortcomings in their data collection and preprocessing needs to be further investigated with more observational data. Figure 10b shows the temporal variation of simulated LAI and soil moisture over the southwestern U.S. Their variability is very consistent, and the correlation coefficient is 0.78. However, over all of NA, the correlation between LAI and soil moisture is low and not significant because during the 1970s and the early 1980s, the relationship seems very weak (not shown), leading to the overall low correlations. Because the soil moisture in this study is a model product, more realistic soil moisture data are desired to investigate this issue further.

6. Conclusions

In this study, we apply the 2-D SSiB4/TRIFFID model that is driven by meteorological forcing and compare the model results with satellite-derived data sets to investigate the dominant factors affecting quasi-equilibrium vegetation status, to assess the biophysical and dynamic vegetation model's ability to simulate vegetation spatial distribution and temporal variability over NA for the past 60 years using observational data, and to identify the most important relationships between NA vegetation and climate.

The photosynthesis optimum temperature (POT), leaf drop threshold temperatures (TOFF), and completion coefficients in the LV equation have been identified as factors that have major impact on the vegetation spatial distribution and the attainment of quasi-equilibrium status in SSiB4/TRIFFID. TOFF will affect how large the area of PFT migration will be under global warming scenarios; the uncertainties in climate forcing and model parameters can greatly influence the simulation of vegetation distribution under climate change conditions. Meanwhile, the fact that vegetation competition coefficients affect quasi-equilibrium conditions suggests the importance of including biotic effects in dynamical vegetation modeling. Despite the high correlation between LAI and soil moisture in the western U.S., we still have difficulty in accurately reproducing the dominant types over the southwestern and central U.S., which may suggest that the model has weakness in producing the existing mechanism of soil moisture-vegetation feedback and handling two possible stable states in arid regions as suggested by *D'Odorico et al.* [2007].

SSiB4/TRIFFID can better reproduce the features of NA distributions of dominant vegetation types, the vegetation fraction, and LAI, including its seasonal, interannual, and decadal variability when compared with satellite-derived products. The NA LAI shows an increasing trend after the 1960s likely responding to increased CO_2, overall warming, and regional precipitation changes as suggested by *Piao et al.* [2006] for Northern Hemisphere greening.

Both simulated and satellite-derived LAIs have the strongest correlations with air temperature at northern middle to high latitudes in spring through their effect on photosynthesis and phenological processes. During

the summer, the areas with positive correlations retreat northward. Meanwhile, in southwestern dry lands, negative correlations between LAI and temperature appear due to the heat stress and moisture stress there during the summer. Furthermore, there are also positive correlations between soil wetness and LAI, which increases from spring to summer. The effects of increasing moisture from 1960 to 1980 and the subsequent effect of the severe drought during 1987–1992 and the last decade in the southwestern U.S. on vegetation are evident from the simulated and satellite-derived LAIs.

The dynamic vegetation models that were originally developed from paleoclimate studies for very long time scales have recently been introduced to decadal- to century-scale studies. The recent published papers with multidynamic vegetation models [*Anav et al.*, 2013; *Murray-Tortarolo et al.*, 2013; *Bao et al.*, 2015] have consistently shown that current dynamic vegetation models have serious weaknesses in reproducing the observed vegetation conditions and have contributed to a large bias in decadal climate simulations. The model evaluations/calibrations using observational data, such as was done in PILPS, have greatly propelled biophysical model development and related climate research in past decades. Considering that the dynamic vegetation models have been and will be used for the future projection, it is imperative to develop better ecological and biophysical understanding of the vegetation dynamics and their interaction with climate at interannual and decadal scales. Recently available observational data from both satellite observations and field measurements provide great opportunity to conduct such research. This paper is a prototype research in this direction, and more studies with different models and focusing on different regions are necessary to achieve a comprehensive understanding on this subject.

References

Alessandri, A., and A. Navarra (2008), On the coupling between vegetation and rainfall inter-annual anomalies: Possible contributions to seasonal rainfall predictability over land areas, *Geophys. Res. Lett.*, *35*, L02718, doi:10.1029/2007GL032415.

Anav, A., G. Murray-Tortarolo, P. Friedlingstein, S. Sitch, S. Piao, and Z. Zhu (2013), Evaluation of land surface models in reproducing satellite derived leaf area index over the high-latitude Northern Hemisphere. Part II: Earth system models, *Remote Sens.*, *5*, 3637–3661, doi:10.3390/rs5083637.

Angert, A., S. Biraud, C. Bonfils, C. C. Henning, W. Buermann, J. Pinzon, C. J. Tucker, and I. Fung (2005), Drier summers cancel out the CO_2 uptake enhancement induced by warmer springs, *Proc. Natl. Acad. Sci. U.S.A.*, *102*, 10,823–10,827.

Arora, V. K., and G. J. Boer (2006), Simulating competition and coexistence between plant functional types in a dynamic vegetation model, *Earth Interact.*, *10*(10), 30, doi:10.1175/EI170.1.

Asharaf, S., and B. Ahrens (2013), Soil-moisture memory in the regional climate model COSMO-CLM during the Indian summer monsoon season, *J. Geophys. Res. Atmos.*, *118*, 6144–6151, doi:10.1002/jgrd.50429.

Bao Y., et al. (2015), Evaluation of CMIP5 Earth system models in reproducing leaf area index and vegetation cover over the Tibetan Plateau, *J. Meteorol. Res.*, *28*, 1041–1060.

Beringer, J. (2010), Ecological climatology: Concepts and applications, 2nd edition – By Gordon B. Bonan, *Geogr. Res.*, *48*, 221–222, doi:10.1111/j.1745-5871.2009.00640.x.

Berry, J., and O. Bjorkman (1980), Photosynthetic response and adaption to temperature in higher plants, *Annu. Rev. Plant Physiol.*, *31*, 491–543.

Bonan, G. B., and S. Levis (2006), Evaluating aspects of the community land and atmosphere models (CLM3 and CAM3) using a dynamic global vegetation model, *J. Clim.*, *19*, 2290–2301.

Bounoua, L., G. J. Collatz, S. O. Los, P. J. Sellers, D. A. Dazlich, C. J. Tucker, and D. A. Randall (2010), Sensitivity of climate to changes in NDVI, *J. Clim.*, *13*, 2277–2292.

Brumbaugh, R., W. Werick, W. Teitz, and J. Lund (1994), Lessons learned from the California drought (1987–1992), Institute for Water Resources, U.S. Army Corps of Engineers, 7701 Telegraph Road, Alexandria, VA 22315–3868.

Carroll, W. D., P. R. Kapeluck, R. A. Harper, and D. H. V. Lear (2002), Background paper: Historical overview of the southern forest landscape and associated resources, in *Southern Forest Resource Assessment*, *Gen. Tech. Rep. SRS-53*, edited by D. N. Wear and J. G. Greis, chap. 24, p. 635, U.S. Department of Agriculture, Forest Service, Southern Research Station, Asheville, N. C.

Claussen, M., and V. Gayler (1997), The greening of the Sahara during the mid-Holocene: Results of an interactive atmosphere-biome model, *Global Ecol. Biogeogr. Lett.*, *6*, 369–377.

Cox, P., R. Betts, C. Jones, S. Spall, and I. Totterdell (2000), Acceleration of global warming due to carbon-cycle feedbacks in a coupled climate model, *Nature*, *408*, 184–187.

Cox, P. M., R. A. Betts, C. D. Jones, S. A. Spall, and I. J. Totterdell (2001), Modelling vegetation and the carbon cycle as interactive elements of the climate system, in *Meteorology at the Millennium*, edited by R. Pearce, pp. 259–279, Academic Press, New York.

Crucifix, M., R. A. Betts, and C. D. Hewitt (2005), Pre-industrial-potential and last glacial maximum global vegetation simulation with a coupled climate-biosphere model: Diagnosis of bioclimatic relationships, *Global Planet. Change*, *45*, 295–312.

D'Odorico, P., K. Caylor, G. S. S. Okin, and T. M. Scanlon (2007), On soil moisture–vegetation feedbacks and their possible effects on the dynamics of dryland ecosystems, *J. Geophys. Res.*, *112*, G04010, doi:10.1029/2006JG000379.

Daly, C., D. Bachelet, J. M. Lenihan, R. P. Neilson, W. Parton, and D. Ojima (2000), Dynamic simulation of tree-grass interactions for global change studies, *Ecol. Appl.*, *10*, 449–469.

Dawdy, D. R., and N. C. Matalas (1964), Statistical and probability analysis of hydrologic data, part III: Analysis of variance, covariance and time series, in *Handbook of Applied Hydrology, A Compendium of Water-Resources Technology*, edited by V. T. Chow, pp. 8.68–8.90, McGraw-Hil, New York.

DeFries, R. S., and J. R. G. Townshend (1994), NDVI-derived land cover classification at a global scale, *Int. J. Remote Sens.*, *15*, 3567–3586.

Delire, C., J. A. Foley, and S. Thompson (2004), Long-term variability in a coupled atmosphere–biosphere model, *J. Clim.*, *17*, 3947–3959.

Di, Z., Q. Duan, W. Gong, C. Wang, Y. Gan, J. Quan, J. Li, C. Miao, A. Ye, and C. Tong (2014), Assessing WRF model parameter sensitivity: A case study with 5-day summer precipitation forecasting in the Greater Beijing Area, *Geophys. Res. Lett.*, *42*, doi:10.1002/2014GL061623.

Dickinson, R. E., M. Shaikh, S. R. Bryant, and L. Graumlich (1998), Interactive canopies for a climate model, *J. Clim.*, *11*, 2823–2836.

Dorman, J. L., and P. J. Sellers (1989), A global climatology of albedo, roughness length and stomatal resistance for atmospheric general circulation models as represented by the Simple Biosphere Model (SiB), *J. Appl. Meteorol.*, *28*, 833–855, doi:10.1175/1520-0450(1989)028<0833:AGCOAR>2.0.CO;2.

Duan, Q., et al. (2006), Model Parameter Estimation Experiment (MOPEX): An overview of science strategy and major results from the second and third workshops, *J. Hydrol.*, *320*, 3–17.

Ecological Stratification Working Group (1996), A national ecological framework for Canada. Agriculture and Agri-Food Canada, Research Branch, Centre for Land and Biological Resources Research, and Environment Canada, State of the Environment Directorate, Ecozone Analysis Branch, Ottawa/Hull. Report and national map at 1:7 500 000 scale.

Fales, S. L., and R. C. Wakefield (1981), Effects of turfgrass on the establishment of woody plants, *Agon. J.*, *73*, 605–610.

Fennessy, M. J., and Y. Xue (1997), Impact of vegetation map on GCM seasonal simulations over the United States, *Ecol. Appl.*, *7*, 22–33.

Foley, J. A., S. Levis, I. C. Prentice, D. Pollard, and S. L. Thompson (1998), Coupling dynamic models of climate and vegetation, *Global Change Biol.*, *4*, 561–579.

Friedl, M. A., D. Sulla-Menashe, B. Tan, A. Schneider, N. Ramankutty, A. Sibley, and X. Huang (2010), MODIS Collection 5 global land cover: Algorithm refinements and characterization of new datasets, *Remote Sens. Environ.*, *114*, 168–182.

Friend, A. D., H. H. Schugart, and S. W. Running (1998), A physiology-based model of forest dynamics, *Ecology*, *74*, 792–797.

Fuhlendorf, S. D., S. Archer, F. E. Smeins, D. M. Engle, and C. A. Taylor Jr. (2008), The combined influence of grazing, fire, and herbaceous productivity on tree–grass interactions, in *Western North American Juniperus Communities: A Dynamic Vegetation Type*, edited by O. W. van Auken, pp. 219–237, Springer, New York.

Hawkins, B. A., et al. (2003), Energy, water and broad-scale geographic patterns of species richness, *Ecology*, *84*, 3105–3117.

Henderson-Sellers, A., Z.-L. Yang, and R. E. Dinkinson (1993), The Project for Intercomparison of Land-Surface Parameterization Schemes (PILPS), *Bull. Am. Meteorol. Soc.*, *74*(7), 1335–1349.

Higgins, S. I., W. J. Bond, and S. W. Trollope (2000), Fire, resprouting and variability: A recipe for grass-tree coexistence in savannna, *J. Ecol.*, *88*, 213–229.

Hughes, J. K., P. J. Valdes, and R. A. Betts (2004) Dynamical properties of the TRIFFID dynamic global vegetation model, Met office, Hadley Centre Tech. Note 56, pp. 23.

Jiang, Y., Q. Zhuang, S. Schaphoff, S. Sitch, A. Sokolov, D. Kicklighter, and J. Melillo (2012), Uncertainty analysis of vegetation distribution in the northern high latitudes during the 21st century with a dynamic vegetation model, *Ecol. Evol.*, *2*, 593–614, doi:10.1002/ece3.85.

Kang, H., Y. Xue, and G. Collatz (2007), Impact assessment of satellite-derived leaf area index datasets using a general circulation model, *J. Clim.*, *20*(6), 993–1015.

Kaufmann, R. K., L. Zhou, R. B. Myneni, C. J. Tucker, D. Slayback, N. V. Shabanov, and J. Pinzon (2003), The effect of vegetation on surface temperature: A statistical analysis of NDVI and climate data, *Geophys. Res. Lett.*, *30*(22), 2147, doi:10.1029/2003GL018251.

Kim, Y. J., and G. L. Wang (2012), Soil moisture-vegetation-precipitation feedback over North America: Its sensitivity to soil moisture climatology, *J. Geophys. Res.*, *117*, D18115, doi:10.1029/2012JD017584.

Kolb, T. E. (1988), Allelopathic effects of Kentucky bluegrass on northern red oak and yellow-poplar, *J. Arboric.*, *14*(11), 281–283.

Krinner, G., N. Viovy, N. de Noblet-Ducoudré, J. Ogée, J. Polcher, P. Friedlingstein, P. Ciais, S. Sitch, and I. C. Prentice (2005), A dynamic global vegetation model for studies of the coupled atmosphere-biosphere system, *Global Biogeochem. Cycles*, *19*, GB1015, doi:10.1029/2003GB002199.

Kutzbach, J. E., G. Bonan, J. Foley, and S. P. Harrison (1996), Vegetation and soil feedbacks on the response of the African monsoon to orbital forcing in the early to middle Holocene, *Nature*, *384*, 623–626.

Latifovic, R., Z.-L. Zhu, J. Cihlar, and C. Giri (2002), Land cover of North America 2000, Natural Resources Canada, Canada Center for Remote Sensing, US Geological Service EROS Data Center.

Levis, S., and G. Bonan (2004), Simulating springtime temperature patterns in the Community Atmosphere Model coupled to the Community Land Model using prognostic leaf area, *J. Clim.*, *17*, 4531–4539.

Li, Q., S. Sun, and Y. Xue (2010), Analyses and development of a hierarchy of frozen soil models for cold region study, *J. Geophys. Res.*, *115*, D03107, doi:10.1029/2009JD012530.

Li, W.-P., Y. Xue, and I. Poccard (2007), Numerical investigation of the impact of vegetation indices on the variability of West African summer monsoon, *J. Meteorol. Soc. Jpn.*, *85A*, 363–383.

Liu, Z., M. Notaro, J. Kutzbach, and N. Liu (2006), An observational assessment of global vegetation–climate feedbacks, *J. Clim.*, *19*, 787–814.

Los, S. O., N. H. Pollack, M. T. Parris, G. J. Collatz, C. J. Tucker, P. J. Sellers, C. M. Malmström, R. S. DeFries, L. Bounoua, and D. A. Dazlich (2000), A global 9-yr biophysical land surface dataset from NOAA AVHRR data, *J. Hydrometeorol.*, *1*, 183–199.

Loveland, T., Z. Zhu, D. Ohlen, J. Brown, B. Reed, and L. Yang (1999), An analysis of the IGBP global land-cover characterization process, *Photogramm. Eng. Remote Sens.*, *65*(9), 1021–1032.

Lu, L., R. A. Pielke Sr., G. E. Liston, W. J. Parton, D. Ojima, and M. Hartman (2001), Implementation of a two-way interactive atmospheric and ecological model and its application to the Central United States, *J. Clim.*, *14*, 900–919.

MacDonald, G. M. (2002), *Biogeography Space, Time and Life*, 518 pp., John Wiley, New York.

MacDonald, G. M. (2010), Climate change and water in southwestern North America special feature: Water, climate change, and sustainability in the Southwest, *Proc. Natl. Acad. Sci.*, *107*, 21,256–21,262, doi:10.1073/pnas.0909651107.

Mayaux, P., E. Bartholome, S. Fritz, and A. Belward (2004), A new land-cover map of Africa for the year 2000, *J. Biogeogr.*, *31*(6), 861–877.

Middleton, N. (2008), *The Global Casino. An Introduction to Environmental Issues*, 4th ed., Arnold, London.

Murray-Tortarolo, G., A. Anav, P. Friedlingstein, S. Sitch, S. Piao, and Z. Zhu (2013), Evaluation of DGVMs in reproducing satellite derived LAI over the Northern Hemisphere. Part I: Uncoupled DGVMs, *Remote Sens.*, *5*, 4819–4838, doi:10.3390/rs5104819.

Nemani, R. R., C. D. Keeling, H. Hashimoto, W. M. Jolly, S. C. Piper, C. J. Tucker, R. B. Myneni, and S. W. Running (2003), Climate-driven increases in global terrestrial net primary production from 1982 to 1999, *Science*, *300*, 1560–1563.

Notaro, M., Z. Liu, and J. W. Williams (2006), Observed vegetation–climate feedbacks in the United States, *J. Clim.*, *19*, 763–786.

Piao, S., P. Friedlingstein, P. Ciais, L. Zhou, and A. Chen (2006), Effect of climate and CO_2 changes on the greening of the Northern Hemisphere over the past two decades, *Geophys. Res. Lett.*, *33*, L23402, doi:10.1029/2006GL028205.

Pimentel, D., R. Zuniga, and D. Morrison (2005), Update on the environmental and economic costs associated with alien-invasive species in the United States, *Ecol. Econ.*, *52*, 273–288.

Pinzon, J., M. E. Brown, and C. J. Tucker (2005), Satellite time series correction of orbital drift artifacts using empirical mode decomposition, in *Hilbert-Huang Transform: Introduction and Applications*, edited by N. Huang and S. S. P. Shen, pp. 167–186, World Scientific, Singapore.

Potter, C., S. Boriah, M. Steinbach, V. Kumar, and S. Klooster (2008), Terrestrial vegetation dynamics and global climate controls in North America: 2001–05, *Earth Interact*, *12*, 1–12, doi:10.1175/2008EI249.1.

Ramankutty, N., and J. A. Foley (1999), Estimating historical changes in land cover: North American croplands from 1850 to 1992, *Global Ecol. Biogeogr.*, *8*, 381–396.

Rehfeldt, G. E., N. L. Crookston, M. V. Warwell, and J. S. Evans (2006), Empirical analyses of plant-climate relationships for the western United States, *Int. J. Plant Sci.*, *167*(6), 1123–1150.

Sage, R. F., and D. S. Kubien (2007), The temperature response of C3 and C4 photosynthesis, *Plant Cell Environ.*, *30*, 1086–1106.

Scheller, R. M., J. B. Domingo, B. R. Sturtevant, J. S. Williams, A. Rudy, E. J. Gustafson, and D. J. Mladenoff (2007), Design, development, and application of LANDIS-II, a spatial landscape simulation model with flexible temporal and spatial resolution, *Ecol. Model.*, *201*, 409–419.

Sheffield, J., G. Goteti, and E. F. Wood (2006), Development of a 50-yr high-resolution global dataset of meteorological forcings for land surface modeling, *J. Clim.*, *19*(13), 3088–3111.

Silvertown, J. (1987), *Introduction to Plant Population Ecology*, 2nd ed., Longman, Scientific and Technical, London.

Sitch, S., et al. (2003), Evaluation of ecosystem dynamics, plant geography and terrestrial carbon cycling in the LPJ Dynamic Global Vegetation Model, *Global Change Biol.*, *9*, 161–185.

Still, C. J., J. A. Berry, G. J. Collatz, and R. S. DeFries (2003), Global distribution of C3 and C4 vegetation: Carbon cycle implications, *Global Biogeochem. Cycles*, *17*(1), 1006, doi:10.1029/2001GB001807.

Taiz, L., and E. Zeiger (2010), *Plant Physiology*, 5th ed., 782 pp., Sinauer Associates, Sunderland Mass.

Wang, G., E. A. B. Eltahir, J. A. Foley, D. Pollard, and S. Levis (2004), Decadal variability of rainfall in the Sahel: Results from the coupled GENESIS-IBIS atmosphere-biosphere model, *Clim. Dyn.*, *22*, 625–637.

Wang, W., B. T. Anderson, D. Entekhabi, D. Huang, R. K. Kaufmann, C. Potter, and R. B. Myneni (2006), Feedbacks of Vegetation on Summertime Climate Variability over the North American Grasslands. Part II: A Coupled Stochastic Model, *Earth Interact.*, *10*, 1–30.

Wang, X., S. Piao, P. Ciais, J. Li, P. Friedlingstein, C. Koven, and A. Chen (2011), Spring temperature change and its implication in the change of vegetation growth in North America from 1982 to 2006, *Proc. Natl. Acad. Sci. U.S.A.*, *108*(4), 1240–1245.

Woodward, F. I., M. R. Lomas, and C. K. Kelly (2004), Global climate and the distribution of plant biomes, *Philos. Trans. R. Soc. London, Ser. B*, *359*, 1465–1476.

Xue, Y. (1997), Biosphere feedback on regional climate in tropical North Africa, *Q. J. R. Meteorol. Soc.*, *123*, 1483–1515.

Xue, Y., P. J. Sellers, J. L. Kinter III, and J. Shukla (1991), A simplified biosphere model for global climate studies, *J. Clim.*, *4*, 345–364.

Xue, Y., M. J. Fennessy, and P. J. Sellers (1996), Impact of vegetation properties on U.S. summer weather prediction, *J. Geophys. Res.*, *101*(D3), 7419–7430, doi:10.1029/95JD02169.

Xue, Y., H.-M. H. Juang, W. Li, S. Prince, R. DeFries, Y. Jiao, and R. Vasic (2004), Role of land surface processes in monsoon development: East Asia and West Africa, *J. Geophys. Res.*, *109*, D03105, doi:10.1029/2003JD003556.

Xue, Y., H. Deng, and P. M. Cox (2006), Testing a coupled biophysical/dynamic vegetation model (SSiB-4/TRIFFID) in different climate zones using satellite-derived and ground-measured data, 86th AMS Annual Meeting, 18th Conference on Climate Variability and Change. [Available at https://ams.confex.com/ams/Annual2006/webprogram/Paper101721.html.]

Xue, Y., F. De Sales, R. Vasic, C. R. Mechoso, S. D. Prince, and A. Arakawa (2010), Global and temporal characteristics of seasonal climate/vegetation biophysical process (VBP) interactions, *J. Clim.*, *23*, 1411–1433.

Zaehle, S., S. Sitch, B. Smith, and F. Hatterman (2005), Effects of parameter uncertainties on the modeling of terrestrial biosphere dynamics, *Global Biogeochem. Cycles*, *19*, GB3020, doi:10.1029/2004GB002395.

Zeng, F.-W., G. J. Collatz, J. E. Pinzon, and A. Ivanoff (2013), Evaluating and quantifying the climate-driven interannual variability in Global Inventory Modeling and Mapping Studies (GIMMS) Normalized Difference Vegetation Index (NDVI3g) at global scales, *Remote Sens.*, *5*, 3918–3950, doi:10.3390/rs5083918.

Zeng, N., H. Qian, C. Roedenbeck, and M. Heimann (2005), Impact of 1998–2002 midlatitude drought and warming on terrestrial ecosystem and the global carbon cycle, *Geophys. Res. Lett.*, *32*, L22709, doi:10.1029/2005GL024607.

Zeng, X. D., X. Zeng, and M. Barlage (2008), Growing temperate shrubs over arid and semiarid regions in the Community Land Model–Dynamic Global Vegetation Model, *Global Biogeochem. Cycles*, *22*, GB3003, doi:10.1029/2007GB003014.

Zhan, X., Y. Xue, and G. J. Collatz (2003), An analytical approach for estimating CO_2 and heat fluxes over the Amazonian region, *Ecol. Model.*, *162*, 97–117.

Zhang, X., et al. (2010), Drought-induced vegetation stress in southwestern North America, *Environ. Res. Lett.*, *5*, 024008, doi:10.1088/1748-9326/5/2/024008.

Zhou, L., R. K. Kaufmann, Y. Tian, R. B. Myneni, and C. J. Tucker (2003), Relation between interannual variations in satellite measures of northern forest greenness and climate between 1982 and 1999, *J. Geophys. Res.*, *108*(D1), 4004, doi:10.1029/2002JD002510.

Zhu, Z., J. Bi, Y. Pan, S. Ganguly, A. Anav, L. Xu, A. Samanta, S. Piao, R. R. Nemani, and R. B. Mynenim (2013), Global data sets of vegetation leaf area index (LAI)3g and fraction of photosynthetically active radiation (FPAR)3g derived from Global Inventory Modeling and Mapping Studies (GIMMS) Normalized Difference Vegetation Index (NDVI3g) for the period 1981 to 2011, *Remote Sens.*, *5*, 927–948.

Zribi, M., T. Paris Anguela, B. Duchemin, Z. Lili, W. Wagner, S. Hasenauer, and A. Chehbouni (2010), Relationship between soil moisture and vegetation in the Kairouan plain region of Tunisia using low spatial resolution satellite data, *Water Resour. Res.*, *46*, W06508, doi:10.1029/2009WR008196.